

11. SITE 1117¹

Shipboard Scientific Party²

SITE 1117

Hole 1117A (RCB):

9°46.526'S, 151°32.945'E; 1663.2 mbsl
0–111.1 mbsf cored; 6.42 m recovered (6%)

Hole 1117B (RCB):

9°46.527'S, 151°32.951'E; 1663.2 mbsl
0–9.5 mbsf cored; 0.05 m recovered (0.5%)

Hole 1117C (RCB):

9°46.520'S, 151°32.943'E; 1663.2 mbsl
0–9.5 mbsf cored; 1.05 m recovered (11.1%)

Site 1117 is on the upper slope of the northern flank of Moresby Seamount, 3.5 km to the northwest of Site 1114. It was a successful attempt to bare-rock spud into, and drill through, the main detachment fault where it crops out.

The base of the cored section consists of a noncumulate, quartz-magnetite gabbro that passes upward into brecciated and then mylonitized equivalents, with a fault gouge at the surface. The upward-increasing shearing and alteration confirm that the northern flank of the seamount is an outcropping fault surface. The first undeformed gabbro occurs at 86 mbsf, but brecciated gabbro was found deeper in the section, at 96 mbsf. Therefore, the minimum thickness of the shear zone preserved within the footwall is about 100 m.

In the surficial core we recovered 4 m of soft, light-colored, clayey material with a soapy feel, interpreted as a fault gouge. This material contains talc, chlorite, calcite, ankerite, and serpentine, which is consistent with hydrothermal alteration of the underlying deformed gabbro. It has low porosity (~30%), bulk density of ~2.2 g·cm⁻³, unconfined compressive strength in the range of 65–90 kPa, thermal conductivities of 1.3–1.8 W·m⁻¹·°C⁻¹, and transverse sonic velocities of

¹Examples of how to reference the whole or part of this volume.

²Shipboard Scientific Party addresses.

~2 km·s⁻¹. These physical properties strongly contrast with those common to near-seafloor deposits and to the gabbro protolith below (porosity 3%, bulk density 2.76 g·cm⁻³, thermal conductivity up to 3.8 W·m⁻¹·°C⁻¹, and sonic velocity 6.0–6.4 km·s⁻¹). Although the fault gouge has been exposed at the seafloor, its characteristics still reflect its deformational origin. The shape parameter of the ellipsoid of magnetic susceptibility ($T = 0.2\text{--}0.8$) indicates an oblate magnetic fabric and the degree of anisotropy of the magnetic susceptibility is maximum in the fault gouge ($P_j = 1.1\text{--}1.2$), both indicative of flattening as a result of high shear strain.

The deformation textures in the gabbro range from brecciated to cataclastic to mylonitic, almost totally obscuring the initial subautomorphic texture. Mylonite clasts recovered down to 57 mbsf show a well-developed foliation with S-C structures. Within the foliation, the association of epidote-rich and very fine grained layers of quartz, epidote, and chlorite reveals greenschist facies conditions during deformation. Asymmetrical fibrous quartz pressure shadows present around pyrite also attest to syntectonic metamorphism. The gabbro between 62 and 86 mbsf shows evidence of increasing brecciation upward, passing progressively to the mylonite. Quartz + epidote veins, reoriented parallel to the foliation in the mylonite, suggest that the brecciation was assisted by silica-rich fluids. Late veins of epidote and calcite cut the rock, attesting to more carbonate-rich fluids in the late stage of shearing. Late alteration, associated with fluid flow within the shear zone, has produced chlorite, talc, and fibrous amphibole replacing primary plagioclase and clinopyroxene.

The mineralogy and texture of the gabbro are similar to those of high-level gabbros occurring in ophiolites. These gabbros, together with the presence of dolerites reminiscent of a sheeted dolerite complex at Site 1114, suggest that Moresby Seamount may be part of an ophiolitic complex exhumed by extension along the northward-dipping low-angle normal fault bounding the seamount to the north.

OPERATIONS

Transit to Site 1117

After finishing operations at Site 1116, we began the transit to Site 1117A in dynamic positioning mode. During the transit, a rotary core barrel (RCB) coring bottom-hole assembly (BHA) with a mechanical bit release (MBR) was assembled. Because the seafloor at Site 1117 was expected to be exposed metamorphic rocks with minimal talus, we used a C-7 core bit that was expected to do better in such harsh drilling conditions. As at earlier holes the mechanical drilling jars were verified to be in good working condition and included in the BHA. The drill string, with a core barrel in place, was lowered to a depth of 1113.3 meters below sea level (mbsl). While the pipe was being lowered to the seafloor, the positioning beacon was deployed at 1205 hr and the ship was positioned over the site.

Hole 1117A

The drill pipe was gently lowered until the bit encountered the seafloor at 1163.2 mbsl and we spudded Hole 1117A at 1535 hr on 26 July (Tables [T1](#), [T2](#)). Because hard rock was exposed at the seafloor, the first

T1. Site 1117 coring summary,
p. 36.

T2. Site 1117 coring summary by
section, p. 38.

Hole 1117A

The hole began in a soft, light-colored clayey material, which had a soapy feel and did not contain any obvious gritty particles beyond a few sparse clasts (one of which was sampled for thin section examination [see paragraphs below]). This clayey material was present in the first two cores: Core 1R with a recovery of 33% and Core 2R with recovery <3%, which suggests that the incoherent material had bottomed out near the top of this core. This material was interpreted as fault gouge and was subsequently found, by use of XRF, to consist of a mixture of the following minerals: talc, chlorite, calcite, ankerite, and serpentine (Table T3). In the fault gouge all three main polytypes of serpentine are present—chrysotile, lizardite, and antigorite. From the X-ray diffraction (XRD) analyses there appears to be a systematic distribution of these mineral types with depth throughout the gouge. Quartz and amphibole are present only in the deepest sample (Section 2R-CC). Talc is almost ubiquitous and chrysotile is present throughout most of Core 1R, whereas calcite and chlorite are present in most samples and also in Section 2R-CC. Antigorite is present only in the uppermost sample and lizardite only in one of the deeper intervals. We assume that differing mineralogical compositions are reflected in the color banding observed in the core (Fig. F2), although this assumption has not been tested. Minerals of the group talc-serpentine-chlorite are common as alteration products of mafic and ultramafic rocks (Deer et al., 1982), suggesting that the protolith for this material can be expected to fall within these compositional types, which is confirmed by fresher material from deeper in the hole (see description below).

This fault gouge contains very sparse, random clasts as noted above. These consist of black, shiny material reminiscent in hand specimen of glass. However, thin-section examination shows that they consist largely of talc with chlorite, calcite, and magnetite. Although not completely homogeneous, these clasts do not seem to contain any clear information on the structure of the protolith.

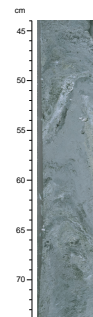
Continuing downward, the next sectioned rock (Core 2R) also consists of chlorite and talc with accessory magnetite. It has a distinct structure, which may be reflecting the original texture of the protolith. This consists of patches of chlorite, 0.5–1.0 cm in diameter, surrounded by fibrous amphibole possibly of the tremolite-actinolite group (Fig. F3). Lath-shaped bodies may be pseudomorphs after original plagioclase, although this could not be substantiated.

The two thin sections from Core 3R show a similar mineral assemblage and, again, a texture that may be reflecting the original protolith, in spite of the fact that replacement has been 100%.

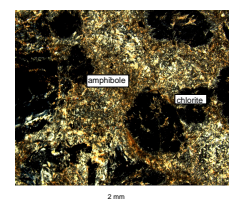
At 57 mbsf (Section 7R-1) true cohesive metamorphic rocks were recovered, various types of mylonites and cataclasites showing pervasive shearing. They are epidote-rich rocks with layers of quartz, epidote, and latest calcite-rich veins. Sulfides (precise nature not determined) are present in small amounts, either in veins or sporadically distributed. Similar mylonites and cataclasites are found downward to Core 11R, where gabbro makes an appearance. The metamorphic rocks fall into the general category of fault rocks. Mineralogically they are composed of epidote, quartz, chlorite, calcite, and variable amounts of finely comminuted material, which is not resolvable under the microscope. The amount of clasts varies widely, so that some rocks with many clasts are termed breccias, whereas others have only small amounts of clasts and consist largely of the finely crushed material. These finer grained rocks

T3. XRD identification of minerals in fault gouge, p. 40.

F2. Core containing fault gouge, p. 14.



F3. Sample composed of secondary minerals, p. 15.



are either mylonites or cataclasites. The former have a strong directional fabric, for example, the sample from Section 9R-1, at ~66 mbsf, where foliation planes within the mylonite are marked by chlorite layers (Fig. F4). This rock also has recognizable angular clasts of clinopyroxene, whereas another rock has clasts of plagioclase, thought to be residual from the protolith. Other rocks (Fig. F5) are cataclasites with no directional fabric. Some are traversed by zones where the crushing is so extreme that the amount of recognizable clasts is so low as to warrant the terms “ultracataclasite” and “ultramylonite” (see “Igneous and Metamorphic Petrology,” p. 9, in the “Explanatory Notes” chapter). Both angular and lenticular clasts consist of epidote and/or quartz, which may result from boudinaged layers formed early in the metamorphism by hydrothermal alteration, or quartz, plagioclase, and pyroxene, which are residual from the gabbro protolith. All these rocks are traversed by late-stage veins of calcite, quartz, and epidote, sometimes with sulfides.

By a depth of 85 mbsf (Section 11R-1), relatively fresh quartz gabbro (Figs. F6, F7, F8) was recovered with a grain size up to ½ cm and a hypidiomorphic texture. Feldspar is still largely sericitized, although remaining anisotropic, indicating that alteration is only partial. The rocks contain up to 10% quartz.

Below this in Section 12R-1 (~95 mbsf) brecciated gabbro was again recovered. This rock has a large amount of chlorite and epidote with fresh plagioclase, which allows the protolith to be identified as gabbro, although all the pyroxene has been replaced. As in previous cases, this rock is cut by late-stage epidote-quartz veins. It has no directional fabric and is termed a protocataclasite because the amount of clasts is high.

The deepest samples, from Section 13R-1 and 14R-1 (105 mbsf), are relatively fresh gabbros, similar to those mentioned above. A description of the gabbros follows with indications as to their affinities based on their mineralogy, texture, and setting.

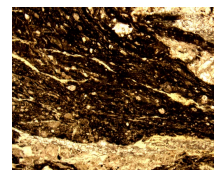
The gabbros are coarse grained (maximum crystal sizes observed were ~8 mm), although there are probably considerable variations in grain size and a suspicion of this variability was gained from the sparse material available (Figs. F6, F7, F8). No directional fabrics or structures (such as layering or lamination) have been observed and the fabric is not that of a cumulate gabbro. Clinopyroxene is largely fresh, plagioclase is altered (clouded by fine micaceous material, although sometimes the outer rims are fresh), and relatively large amounts of quartz are present, sometimes as clear anhedral grains and sometimes in patches of granophyre (Fig. F7B). Spectacular dendritic magnetite crystals were observed in one sample, although all have skeletal magnetite. In one sample, the clinopyroxene is undergoing alteration to tremolite-actinolite. Other altered material in the gabbros is now represented by chlorite, although its original nature could not be determined.

In summary, these are relatively evolved magnetite-quartz gabbros, which have presumably crystallized in place because they have a distinctly non-cumulate texture.

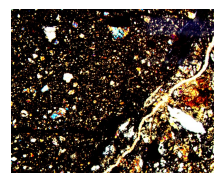
Holes 1117B and 1117C

Section 180-1117B-1R-1 contained three pebbles of sheared mylonitic rock, which have a glassy appearance on uncut surfaces, likely caused by the previously described alteration to talc and other finely divided layer silicates. None of these rocks were sectioned or analyzed by XRF. Two thin sections were made from the sparse recovery from

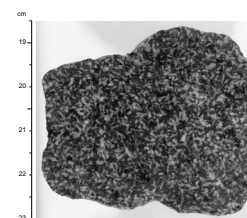
F4. Mylonite, p. 16.



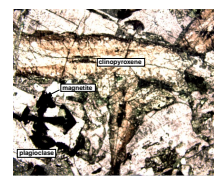
F5. Cataclasite and breccia, p. 17.



F6. Fragment of gabbro, p. 18.



F7. Gabbro with plagioclase, clinopyroxene, and magnetite, p. 19.



F8. Gabbro with clouded plagioclase, p. 21.



Hole 1117C. One is a sample of mylonite, very similar to those already described except that the clasts make up only a relatively small part of the rock, and therefore, it would be specified as an ultramylonite. The other sample consists of a very fine grained material, which could not be identified optically, but does not appear to be the same talc-chlorite mix found above. This rock is traversed by two vein systems: an earlier one filled with quartz, and a later one containing a mixture of quartz, chlorite, and sericite.

Chemistry

Chemical analyses by XRF for major and trace elements of two analyzed gabbros are shown in Tables T4 and T5. The two quartz gabbros are significantly different in composition, particularly in terms of Fe_2O_3 , TiO_2 and $\text{Fe}_2\text{O}_3/\text{MgO}$ ratio, an observation very common in such rocks that are not liquid compositions. An analysis of a ferrogabbro from the Samail Ophiolite (Lippard et al., 1986) has been included for comparative purposes and it can be observed that many of the elements fall in the same range.

Features common to the two gabbro samples are the relatively low TiO_2 and K_2O and similar SiO_2 and MgO contents. There is little doubt that we are dealing with similar rock types, but the Semail Ophiolite samples appear to be generally higher in Zr, Cr, and V and lower in Cu. All samples recovered from Site 1117 are altered, the quartz gabbros only marginally, the exact significance of these differences is not clear. The brecciated quartz gabbro (Sample 180-1117A-12R-1, 11–13 cm) appears to be similar to the quartz gabbros.

A distinctly different composition is shown by the chlorite-epidote schist (Sample 180-1117A-9R-1, 85–86 cm), which is high in MgO , Ce, Ni, and Cr (spectacularly so) and low in Na_2O . If this rock were derived from the quartz gabbro, it seems that either its protolith was distinctly different from the two analyzed quartz gabbros or that the process was not isochemical.

The fault gouge (Sample 180-1117C-1R-1, 9–10 cm) is very different from any of the others; it is siliceous and poor in both Fe_2O_3 and MgO and high in Ba, Ce, and Rb. The reason for these extreme chemical variations remains obscure.

In summary, the chemical compositions of the quartz gabbros and their mylonitized equivalent are consistent with their origin as a high-level gabbro in an ophiolite complex, although this is in no way specific and other environments are by no means ruled out. The other two rocks analyzed are distinctly different, but whether this is because of different protoliths or to metasomatic alteration is unknown.

Interpretation

These data are consistent with the drill entering a fault zone and continuing through zones of metamorphosed and brecciated material into relatively unaltered gabbro, which was the protolith for the rocks. The metamorphic rocks are of the type and fabric to be expected from intense shearing and fluid flow along a major fault zone.

The gabbro belongs to the noncumulate, quartz-magnetite variety found in a number of settings, including the upper levels of ophiolites, such as at Oman (Pallister and Hopson, 1981) and Troodos (Robertson and Xenophontos, 1994). Ophiolitic, high-level gabbros have the same

T4. XRF results for major elements,
p. 41.

T5. XRF results for trace elements,
p. 42.

features described here: variable grain size, evolved nature (containing quartz and magnetite), presence of zoned minerals (as in the clinopyroxene shown in Fig. F7A), lack directional fabrics or layering, and often show alteration (e.g., of pyroxene to hydrothermal amphibole as shown in Fig. F8). In conjunction with the observations from Site 1114 and to a lesser extent Sites 1110–1113, which show that the top of Moresby Seamount consists largely of dolerites reminiscent of an ophiolitic sheeted dolerite complex, the results are consistent with the hypothesis that this topographic high represents part of an ophiolite complex exhumed by extension along a major fault plane. This interpretation suggests that the gabbros sampled at Site 1117 are the high-level gabbros recognized in other ophiolites.

STRUCTURAL GEOLOGY

Despite the low recovery from the three holes drilled at Site 1117 (~5%), the structures observed in the rocks allow us to define four structural domains (Fig. F9). The four domains are from the top to the bottom: a fault gouge (Domain I) from 0 to 12.37 mbsf in Cores 180-1117A-1R and 2R; a mylonitic zone (Domain II) in Cores 180-1117A-2R through 7R and in Core 180-1117B-1R; a brecciated zone (Domain III) observed in Cores 180-1117A-8R to 12R and in Core 180-1117C-1R; and an undeformed zone (Domain IV) observed at the bottom of Hole 1117A (Cores 180-1117A-13R and 14R). A truly cohesive section was recovered from Cores 180-1117A-13R and 14R (gabbro); the overlap between Domains II and III is because of the presence of a few mylonitic pebbles in the breccia; the overlap of Domains III and IV is because of the presence of a few brecciated zones in the gabbro.

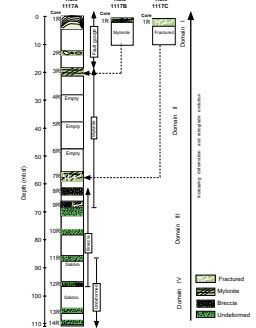
Domain I

Domain I comprises Cores 180-1117A-1R and 2R. Core 180-1117A-1R, from 0 to 12.20 mbsf, recovered 4.07 m of soft, light colored clayey material containing few sparse clasts (see “Hole 1117A,” p. 4). The initial attitude of an obvious preferential orientation in the fault gouge is difficult to assess because it has been folded during coring (Fig. F10). The mineralogy of this zone (pebbles and matrix), defined by XRD and microscope observation, gives a talc-serpentine-chlorite composition with minor quartz and amphibole present at the bottom of the zone (see “Hole 1117A,” p. 4). Core 180-1117A-2R from 12.20 to 12.37 mbsf contains numerous cm-sized pebbles in a clayey material at the boundary between the fault gouge and the underlying igneous basic rocks. This intermediate unit is included in Domain I.

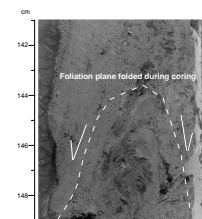
Domain II

In Domain II from 18.60 to 57.07 mbsf (Hole 1117A) the recovered rocks show very well developed anastomosing foliation planes and shear bands (Fig. F11) and fibrous quartz pressure shadows around pyrite (Fig. F12) in greenschist basic rocks (see “Hole 1117A,” p. 4). The foliation plane is defined by the alternation of epidote-rich layers and very fine grained layers made of epidote, quartz, and chlorite assemblages. Below 57.08 mbsf in Hole 1117A and at 0.09 mbsf in Hole 1117B, a few samples have an ultra-mylonitic texture characterized by the transposition of the planar structures where foliation plane and

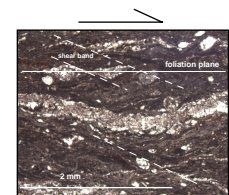
F9. Structural domain distribution in Holes 1117A, 1117B, and 1117C, p. 22.



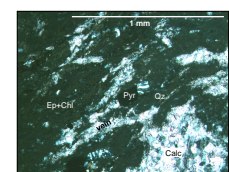
F10. Fault gouge recovered in Hole 1117A, p. 23.



F11. Mylonite with sigmoidal lenses of quartz, p. 24.



F12. Fibrous quartz pressure shadow around pyrite grain, p. 25.



shear bands become parallel (see Fig. F4). In all the samples a network of calcite veins crosscut the foliation plane.

Domain III

Domain III ranges from 61.60 to 96.06 mbsf (Sections 180-1117A-8R-1 to 12R-1) and is defined by the brecciation of gabbroic rock (Fig. F13). It consists of the fragmentation of plagioclase and clinopyroxene present as small clasts in a dark brown matrix made of very fine grained epidote, quartz, and clay assemblages. The intensity of the brecciation increases upward, and the number and size of the relics of clinopyroxene and plagioclase decrease upward. This is related to the presence of the mylonitization at the top of the sequence overprinting the breccia. In one sample (Fig. F14) the relationship between the breccia and the mylonitization of the rocks is demonstrated. The brecciated gabbros from Domain III are crosscut by epidote + quartz and quartz veins (Fig. F15A, F15B); the latter are subsequently reoriented into the mylonite as they form boudinaged quartz + epidote or quartz-rich layers.

Domain IV

Domain IV consists of an undeformed coarse-grained gabbro with no directional fabrics such as layering (F6; see "Hole 1117A," p. 4). This domain ranges from 105.2 mbsf (Section 180-1117A-13R-1) to the bottom of the hole (110.1 mbsf).

Interpretation

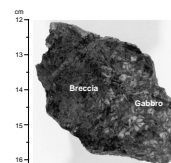
The fresh gabbroic rocks recovered at the bottom of Hole 1117A are thought to be the original basic rock that underwent ductile (mylonitization) to brittle (brecciation, fracturing) deformation and retrograde evolution from middle crustal level (plutonic conditions) to upper continental level (greenschist facies conditions). The tectono-metamorphic evolution could be related to the unroofing of the gabbro during extensional tectonics. Similar evolution has been described for the metadolerite recovered in Hole 1114. Indeed, at these two sites there is a massive brittle deformation (brecciation) associated with the development of greenschist minerals. At Sites 1114 and 1117 we observe the brecciation of the rocks (dolerite and gabbro) at the bottom of the sequence overprinted by a sheared zone giving rise to the development of an intense mylonitic fabric in the rocks. At both sites, the breccia formed by fluid-assisted fracturing (Fig. F16) of the rocks (gabbro and dolerite). At the earliest stage of the deformation and deeper in the gabbroic body, fluid should be siliceous as epidote + quartz occurs in veins. Later during the evolution and shallower in the gabbroic body, the fracturing is associated with carbonate-rich fluids as calcite occurs in veins.

BIOSTRATIGRAPHY

Sample 180-1117A-1R-CC is barren of nannofossils and foraminifers. Cores 180-1117A-2R to 14R and 180-1117B-1R recovered no sediment.

Sample 180-1117C-1R-CC contained a black mudstone pebble. The pebble contains no foraminifers, but it does contain a few moderately preserved nannofossils. The presence of *Discoaster brouweri* and *Pseudomilania lacunosa* restricts the pebble to Pliocene Zones NN14–NN18.

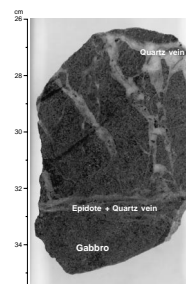
F13. Hand specimen showing development of breccia, p. 26.



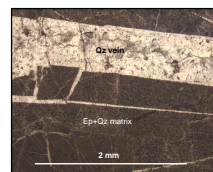
F14. Sheared zone overprinting breccia, p. 27.



F15. Hand specimen with veins fracturing gabbro, p. 28.



F16. Igneous rock fractured during Si-rich fluid circulation, p. 30.



PALEOMAGNETISM

The investigation of magnetic properties at Site 1117 included the measurement of point susceptibilities and remanent magnetization of archive sections from Core 180-1117A-1R, and the measurement of magnetic susceptibility and its anisotropy, acquisition of isothermal remanent magnetization (IRM), decay of anhysteretic remanent magnetization (ARM), and remanent magnetization of discrete samples.

Discrete samples measured were as follows: three samples from Core 180-1117A-1R (metamorphic-derived material interpreted as fault gouge; see “[Hole 1117A](#),” p. 4); one sample from Section 1117A-2R-CC (a clast from unconsolidated metamorphic material); one sample from interval 180-1117A-9R-1 (Piece 17) (epidote breccia); and one sample from interval 180-1117A-11R-1 (Piece 7) (gabbro; see “[Igneous and Metamorphic Petrology](#),” p. 3).

Remanent Magnetization

Measurements of remanent magnetization were made on discrete samples taken from working half core sections (Fig. F17) and on archive sections from Core 180-1117A-1R (Fig. F18).

Initial natural remanent magnetization (NRM) intensities of discrete samples were on the order of 10^{-2} A·m⁻¹ to 10^{-1} A·m⁻¹. Demagnetization behavior of discrete samples from Cores 180-1117A-1R and 2R was erratic with no stable end-point reached (Fig. F17A, F17B). However, demagnetization behavior of samples from Cores 180-1117A-9R and 11R showed a linear decay toward the origin between ~20 and 50 mT on vector plots (Fig. F17C, F17D). Discrete sample data from Core 180-1117A-1R did not generally agree with the long core data (Fig. F18A, F18B).

Intensity of remanent magnetization of sections from Core 180-1117A-1R after AF demagnetization at 20 and 25 mT was on the order of 10^{-3} A·m⁻¹ (Fig. F18A, F18B); inclinations and declinations are shown but are considered unreliable because of the erratic demagnetization behavior of discrete samples. No attempt was made to interpret the data in terms of the magnetic polarity time scale.

Magnetic Susceptibility

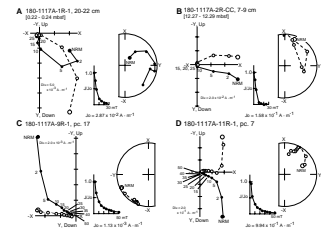
Magnetic susceptibility measurements were made on archive sections of Core 180-1117A-1R as part of the archive multisensor track (AMST) analysis. The AMST susceptibilities (uncorrected for volume) were on the order of 10^{-3} SI (Fig. F19).

Mean susceptibility values and magnetic anisotropy parameters of discrete samples are listed in Table T6. A plot of the shape parameter (T) vs. the degree of anisotropy (P_i) is shown in Figure F20A. All samples showed T values greater than 0, which indicated an oblate magnetic fabric; samples from Core 180-1117A-1R, which recovered only fault gouge (see “[Hole 1117A](#),” p. 4), showed a higher degree of anisotropy than the other samples.

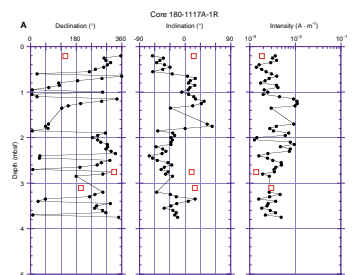
Rock Magnetism

Experiments on the acquisition of IRM and the demagnetization of ARM were conducted on all six discrete samples. The ARMs were

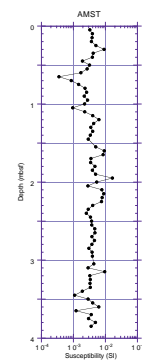
F17. Demagnetization behavior of discrete samples, p. 31.



F18. Plots of declination, inclination, and intensity, p. 32.

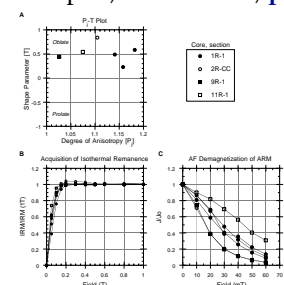


F19. Susceptibility data from AMST measurements, p. 34.



T6. AMS data of discrete samples, Hole 1117A, p. 43.

F20. Rock magnetic data for discrete samples, Hole 1117A, p. 35.



imparted to samples using a 0.05 mT DC field in an AC peak field of 100 mT.

All samples were saturated by 0.2 T during experiments of the acquisition of IRM (Fig. F20B); this suggested the presence of only magnetite in the measured samples. The sample from Section 180-1117A-11R-1 was most resistant to AF demagnetization of ARM, while the samples from Cores 180-1117A-2R and 9R were least resistant to AF demagnetization of ARM (Fig. F20C). Behavior during AF demagnetization of ARM suggested a finer grain size of magnetite in the sample from Core 180-1117A-11R, which was from a gabbro (see "Hole 1117A," p. 4), than in the fault gouge samples (Core 180-1117A-1R). The curves for the two samples of metamorphic clasts from Cores 180-1117A-2R and 9R reflected the largest magnetic grain size.

ORGANIC GEOCHEMISTRY

At Site 1117 the shipboard organic geochemistry consisted of determinations of TOC, inorganic carbon, total carbon, total nitrogen, and total sulfur in addition to the routine hydrocarbon gas safety monitoring procedure. The analytical techniques used are outlined in "Organic Geochemistry," p. 25, in the "Explanatory Notes" chapter.

Volatile Hydrocarbons

Only two headspace gas samples were collected at Site 1117. These contained methane at very low concentrations, 1.9 and 2.3 ppm at 1.5 (Core 180-1117A-1R) and 12.2 mbsf (Core 180-1117A-2R) respectively. No other hydrocarbons were detected.

CaCO₃, Sulfur, Organic Carbon, and Nitrogen

The CaCO₃ contents at Site 1117 ranged between 4.8 and 15.7 wt% (Table T7). Organic carbon was detected in only two samples at 1.35 and 3.88 mbsf in Core 180-1117A-1R and contained 0.12 and 0.23 wt% respectively. Sulfur only occurred in one sample (0.04 wt%, 1.35 mbsf; Table T7). Nitrogen was not detected in any of the samples.

T7. Calcium carbonate, carbon, nitrogen, and sulfur contents, p. 44.

PHYSICAL PROPERTIES

Introduction

Because of the low recovery at Site 1117 only Core 180-1117A-1R was analyzed on the multisensor track (MST). Thermal conductivity and velocity were measured from discrete rock slices or pieces of split core in order to preserve intact fabrics. Unconfined compressive strength was measured in the fault gouge at the top of the recovered succession (Cores 180-1117A-1R and 2R), but no vane shear strength measurements could be conducted. Lack of recovery at Holes 1117B and 1117C prevented acquiring physical properties measurements. All physical properties data collected at Site 1117 are presented in Table T8, except the MST data. A compilation of MST data (in ASCII format) is presented on the accompanying LDEO CD-ROM.

T8. Physical properties measurements, p. 45.

Results of Physical Properties Measurements

Fault gouge material was found to have bulk densities between 2.14 and 2.28 g·cm⁻³. Grain densities range from 2.75 to 2.80 g·cm⁻³. Porosity values are between 28.6% and 32.3%. Pocket penetrometer measurement of unconfined compressive strength yielded values between 65 and 90 kPa. Higher strength was recorded for intervals exhibiting scaly fabrics and micro shear folds. Transverse velocities range from 1992 to 2038 m·s⁻¹. To avoid damage to the fault gouge fabrics with the needle probe, thermal conductivity was taken with the half-space device on the split core face. Results range from 1.32 to 1.75 W·m⁻¹·°C⁻¹.

Selected cubes and a minicore of metadolerite and gabbro were prepared from the recovered section below 18.6 mbsf. Bulk and grain density are 2.76 and 2.82 g·cm⁻³, respectively. Porosity is only 2.95%. Transverse velocities range from 6076 to 6432 m·s⁻¹, whereas longitudinal velocities are 5991 to 6337 m·s⁻¹. Thermal conductivity was found to be highly variable, ranging from 1.15 W·m⁻¹·°C⁻¹ (Section 180-1117R-9R-1) to up to 3.78 W·m⁻¹·°C⁻¹ (Section 180-1117A-12R-1). However, this variation in thermal conductivity may relate to a measurement bias, because the lowest values correspond to the smallest piece of half core.

REFERENCES

- Deer, W.A., Howie, R.A., and Zussman, J., 1982. *An Introduction to the Rock-Forming Minerals* (13th ed.): Harlow (Longman).
- Jelinek, V., 1981. Characterization of the magnetic fabric of rocks. *Tectonophysics*, 79:63-67.
- Lippard, S.J., Shelton, A.W., and Gass, I.G., 1986. *The Ophiolite of Northern Oman*. Geol. Soc. London Mem., 11.
- Pallister, J.S., and Hopson, C.A., 1981. Samail ophiolite plutonic suite: field relations, phase variation, cryptic variation and layering, and a model of a spreading ridge magma chamber. *J. Geophys. Res.*, 86:2593-2644.
- Robertson, A.H.F., and Xenophontos, C., 1993. Development of concepts concerning the Troodos ophiolite and adjacent units in Cyprus. In Prichard, H.M., Alabaster, T., Harris, N.B.W, and Neary, C.R. (Eds.), *Magmatic Processes and Plate Tectonics*. Geol. Soc. Spec. Publ. London, 76:85-119.

Figure F1. Log of Holes 1117A, 1117B, and 1117C showing recovery, rock type, and sample distribution. XRD = position of sample for X-ray diffraction; TSB (“thin section billet”) = position of thin section sample; and XRF = sample for X-ray fluorescence analysis.

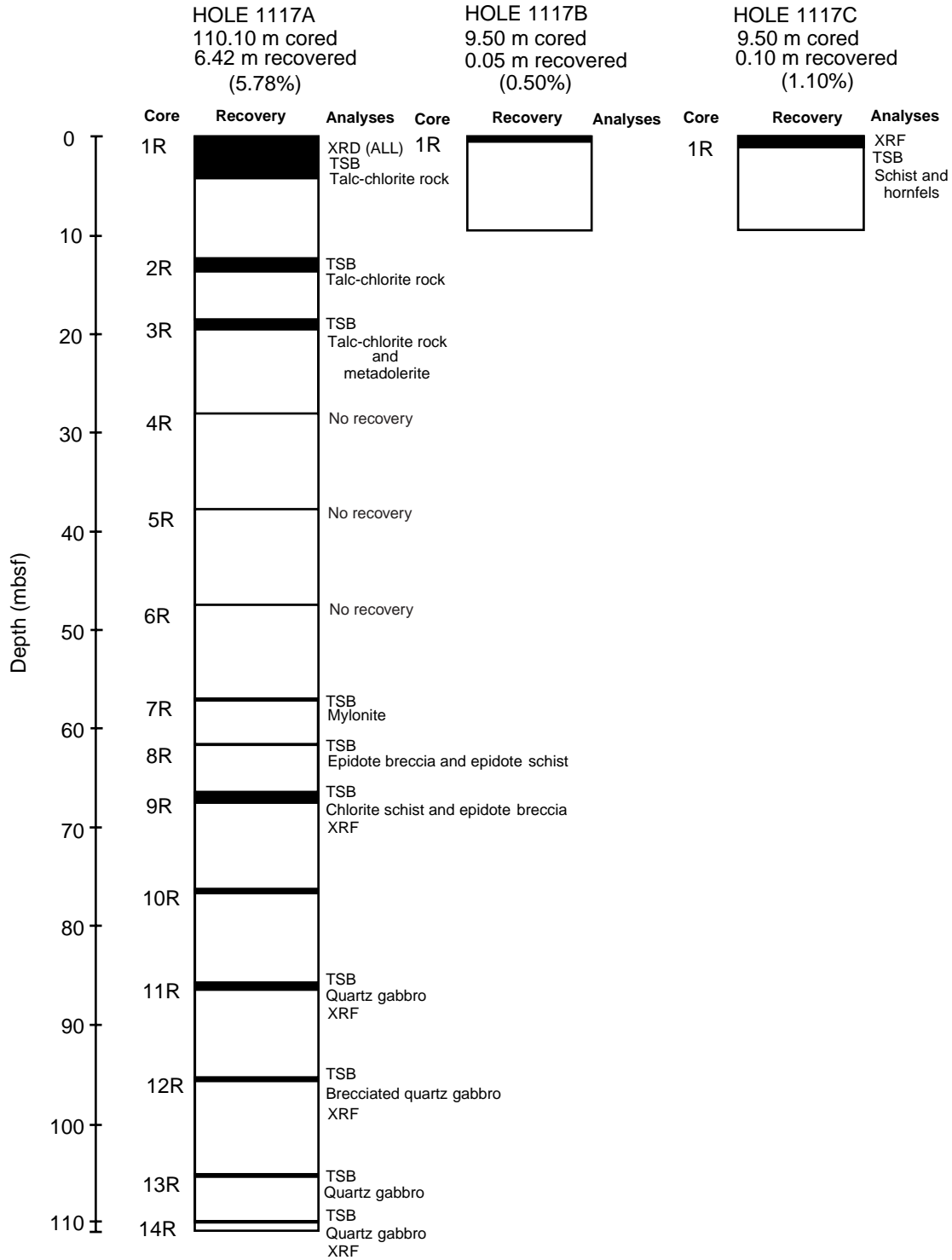


Figure F2. Core containing fault gouge. Original variations in composition (probably caused by varying proportions of the minerals listed in Table T3, p. 40) are shown by color variations and have been very disturbed by drilling (interval 180-1117A-1R-2, 44–74 cm).

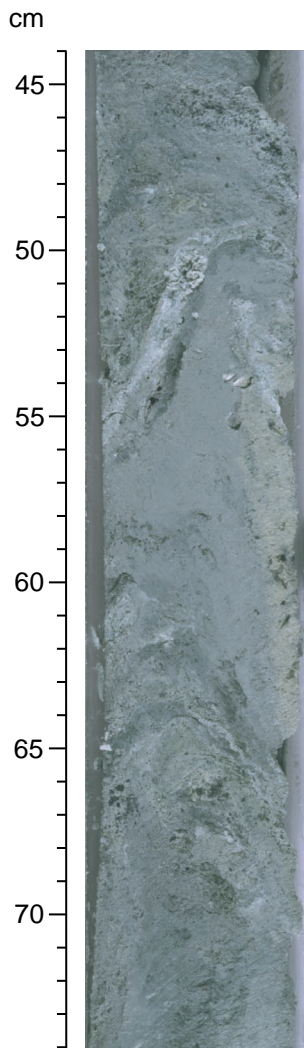
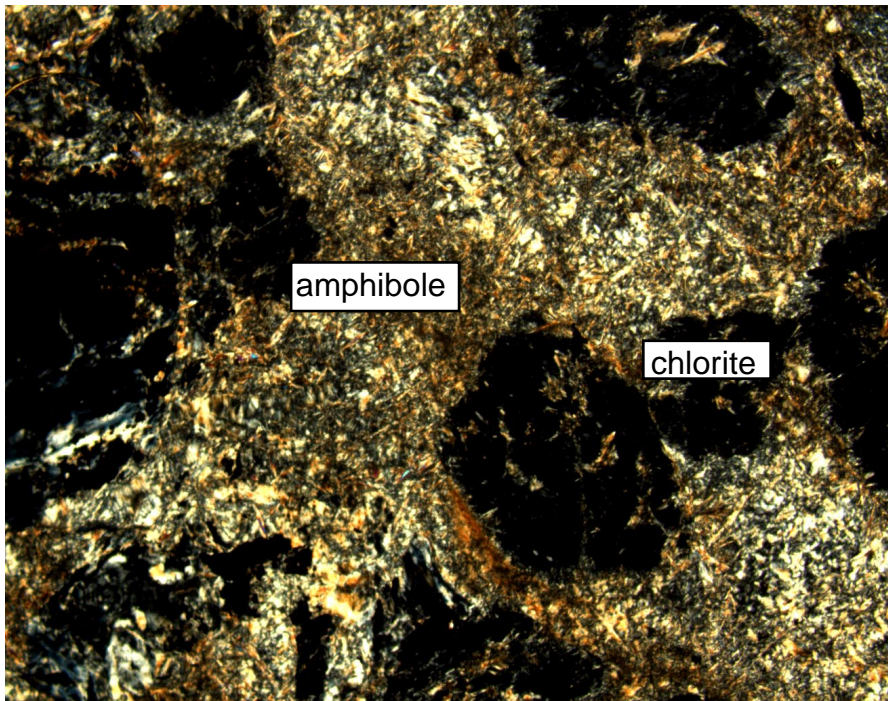
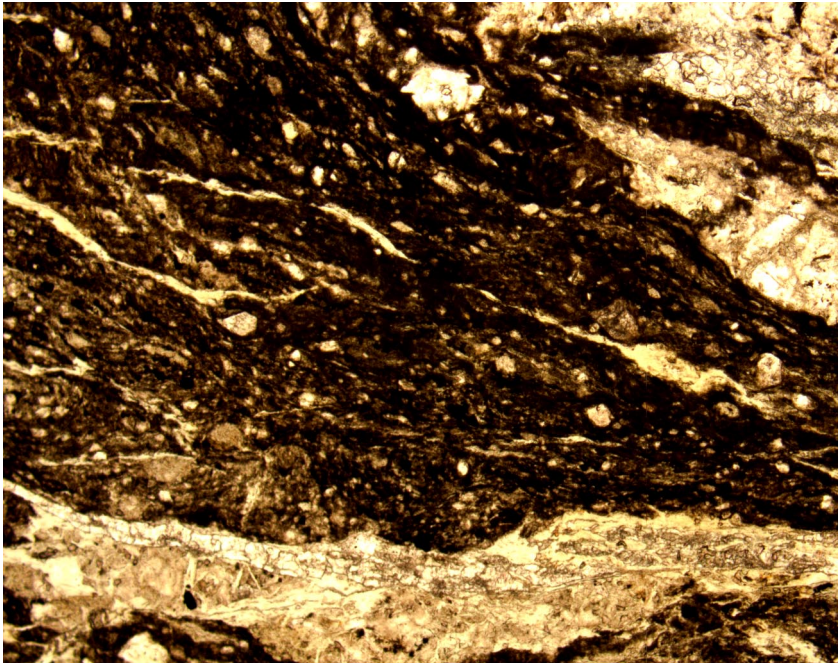


Figure F3. Digital photograph of a sample totally composed of secondary minerals, largely chlorite and amphibole (probably a member of the actinolite-tremolite group). The distribution of these phases may represent the texture of the immediate gabbroic (?) precursor (interval 180-1117A-3R-CC, 3-4 cm).



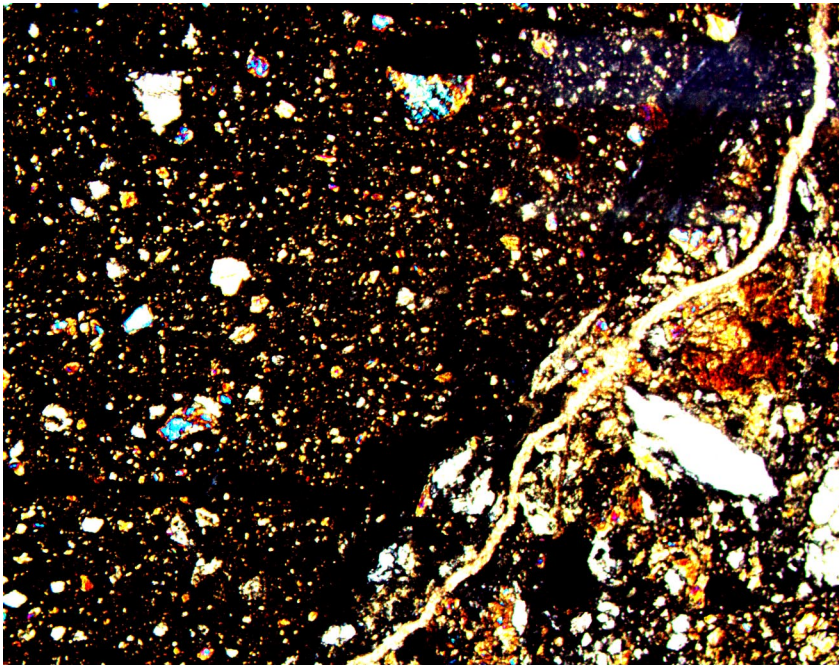
2 mm

Figure F4. Digital photomicrograph of a mylonite. Identifiable material consists of fragments of pyroxene, plagioclase, and quartz. Veins contain calcite, quartz, and chlorite (interval 180-1117A-9R-1 [Piece 4, 15–20 cm]).



2 mm

Figure F5. Digital photomicrograph showing cataclasite in the upper left of the photograph and breccia in the lower right. Identifiable clasts include pyroxene, plagioclase, and epidote (interval 180-1117A-9R-1 [Piece 18, 86–90 cm]).



2 mm

Figure F6. Hand specimen of gabbro fragment showing coarse-grained texture and no layering at the scale of the recovered material (interval 180-1117A-13R-1, 18.5–23 cm).

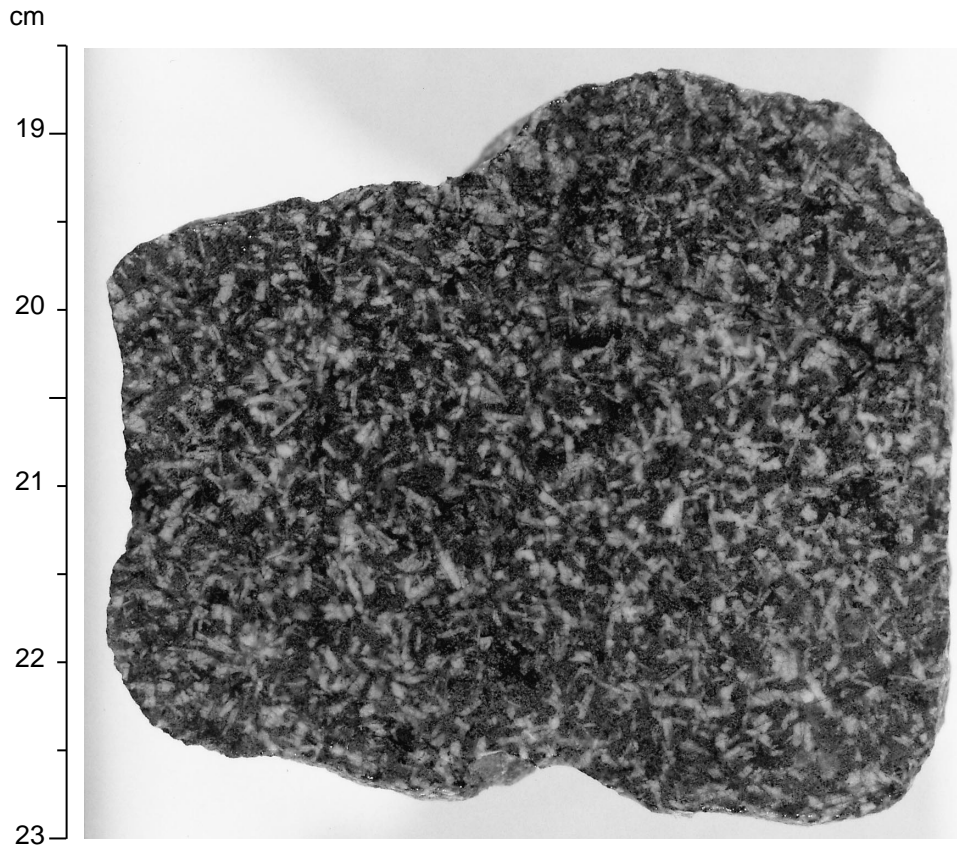
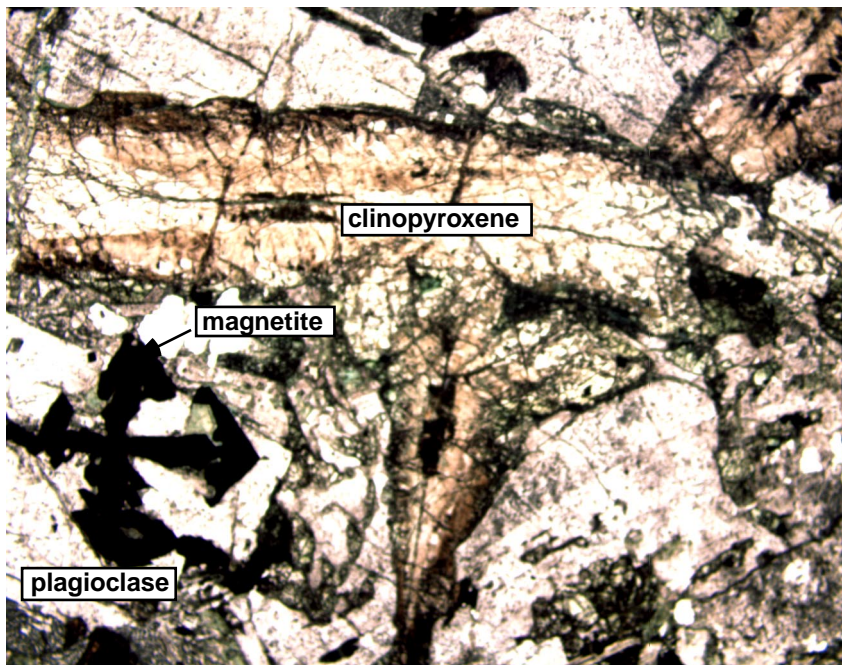
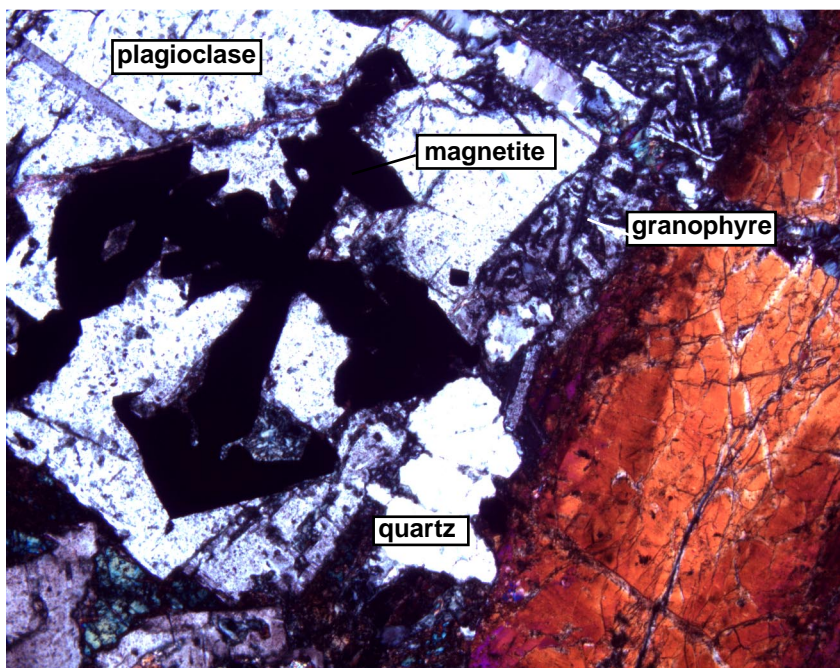


Figure F7. Digital photomicrograph of a gabbro sample. A. Gabbro showing relatively fresh plagioclase, zoned clinopyroxene, and dendritic magnetite (Sample 180-1117A-14R-1 [Piece 4, 13–15 cm]). (Continued on next page.)



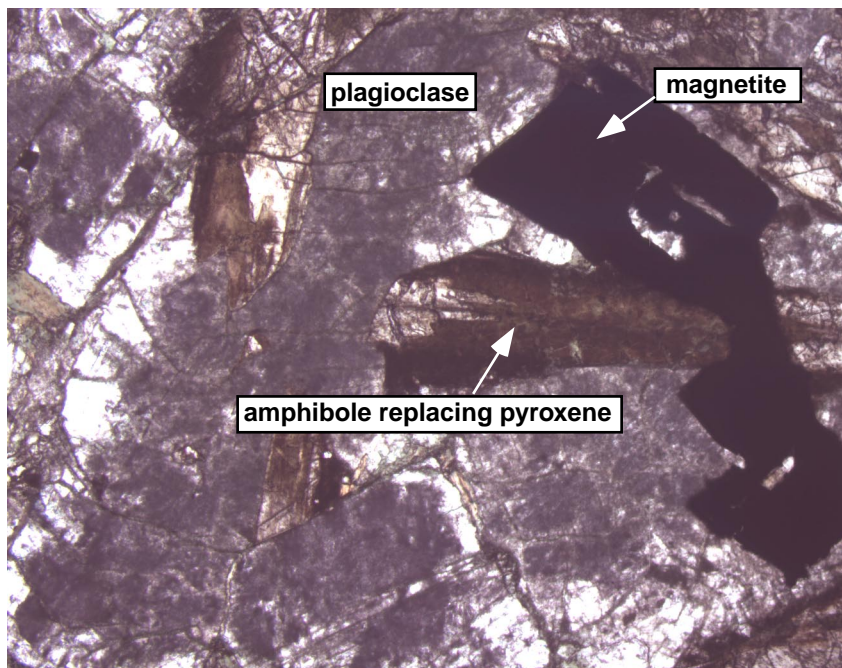
4 mm

Figure F7. (continued). B. Same sample under a higher magnification. The cruciform crystal of magnetite set in fresh plagioclase dominates the left side of the figure. Zoning is clearly seen in the clinopyroxene at the right, and quartz occurs as clear grains or in granophyric intergrowth as marked (Sample 180-1117A-14R-1 [Piece 4, 13–15 cm]).



2 mm

Figure F8. Digital photomicrograph of a gabbro showing clouded plagioclase (some grains have a clear marginal zone) and magnetite. In this rock, partial alteration of clinopyroxene is taking place, leading to an amphibole of the actinolite-tremolite group (Sample 180-1117A-11R-1 [Piece 7, 30–39 cm]).



1 mm

Figure F9. Recovered sequences from Holes 1117A, 1117B, and 1117C showing the structural distribution of Domains I, II, III, and IV. Domain I consists of the fault gouge, Domain II consists of the mylonite, Domain III consists of the breccia, and Domain IV represents the undeformed gabbro at the bottom of Hole 1117A.

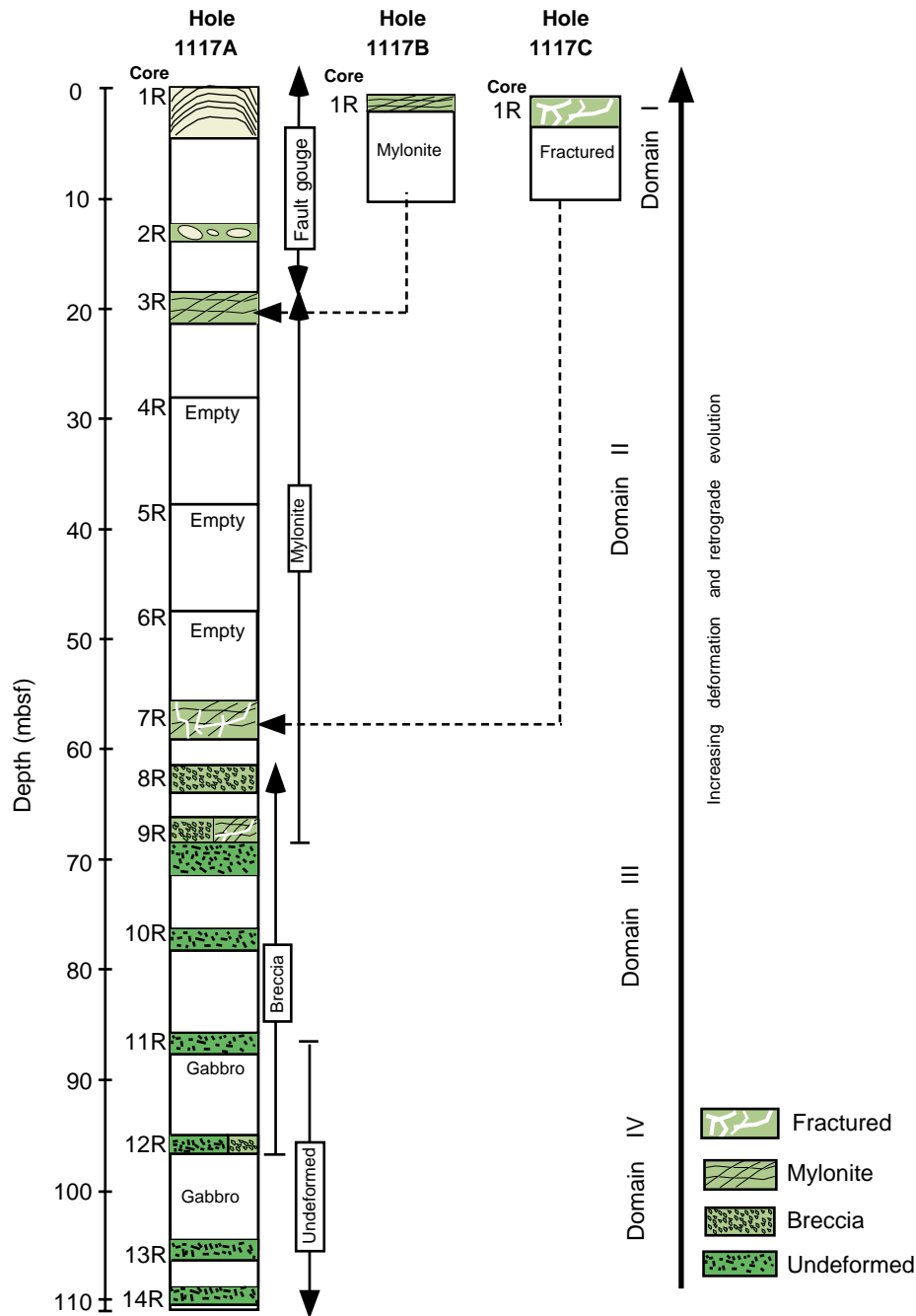


Figure F10. Fault gouge recovered in Hole 1117A, Core 180-1117A-1R. The development of the fold is because of coring deformation overprinting of weakly developed foliation (Sample 180-1117A-1R-2, 141–149 cm).

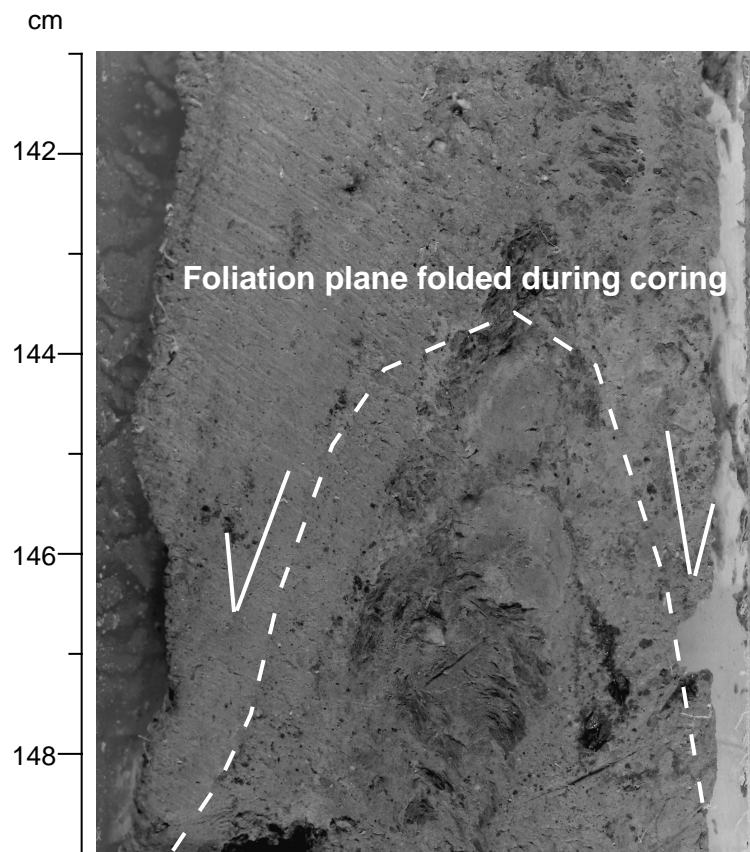


Figure F11. Mylonite with sigmoidal lenses of quartz defining the shear bands. Note the presence of the epidote-rich layer elongated in the foliation plane (Sample 180-1117A-9R-1 [Piece 4, 15–20 cm]).

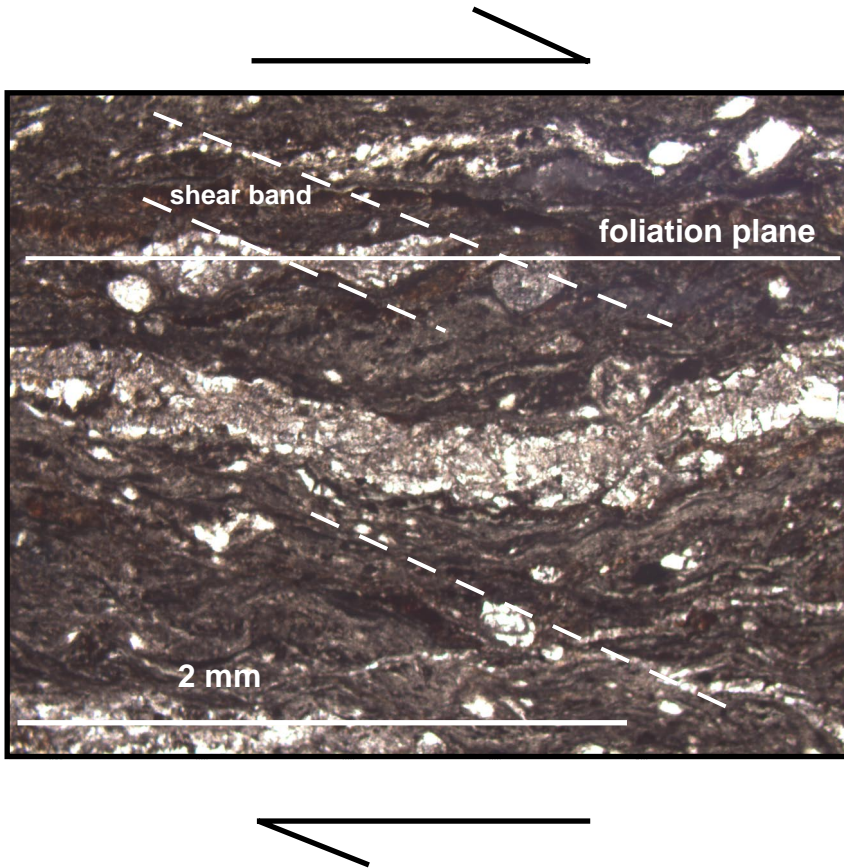


Figure F12. Fibrous quartz pressure shadow around pyrite grain. Occurrence of calcite in veins and in the matrix of the rock replacing previous minerals (Sample 180-1117A-7R-1, 3–4 cm). Pyr = pyrite; Qz = quartz; Ep + Chl = epidote + chlorite; Calc = calcite.

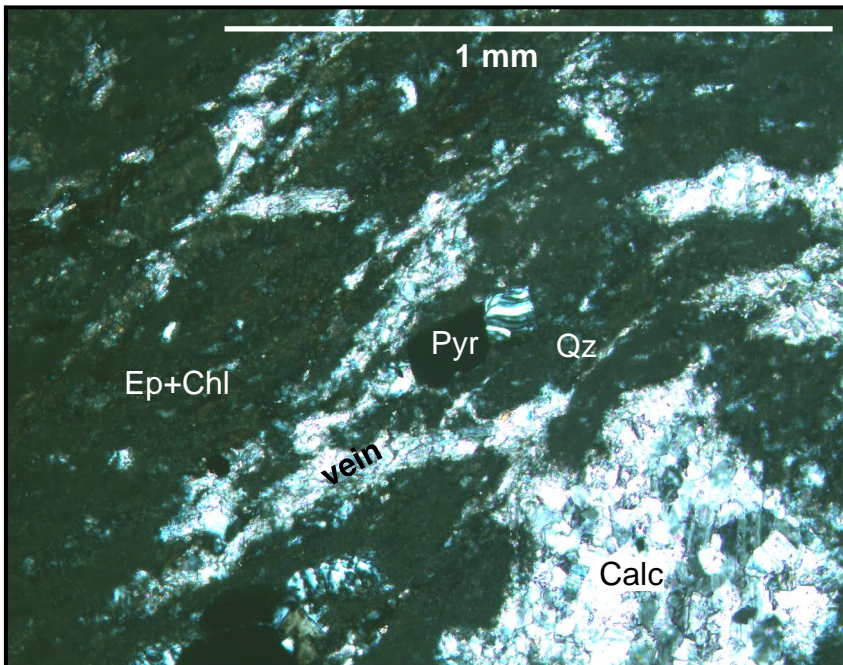


Figure F13. Hand specimen showing the development of the breccia in the gabbro (Sample 180-1117A-14R-1, 12–16 cm).

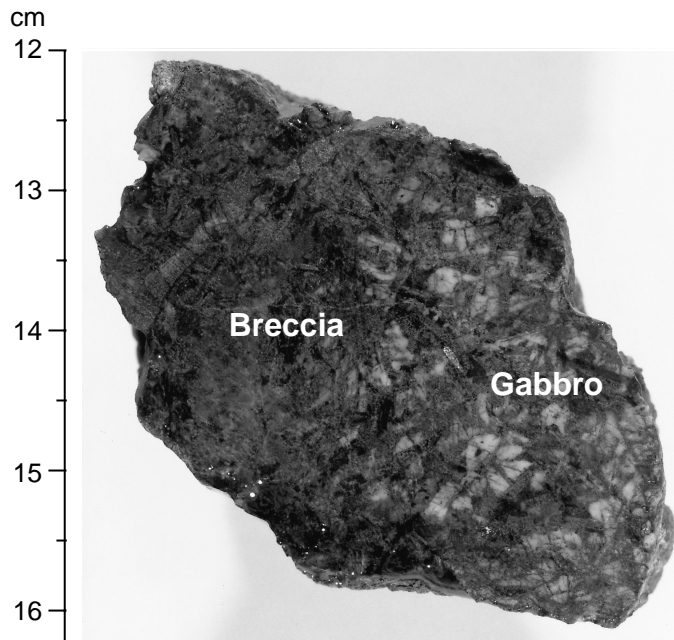


Figure F14. Sheared zone overprinting the breccia, related to the development of a strong mylonitic fabric upward into Hole 1117A (Sample 180-1117A-9R-1 [Piece 10, 86–90 cm]). Cpx = clinopyroxene.

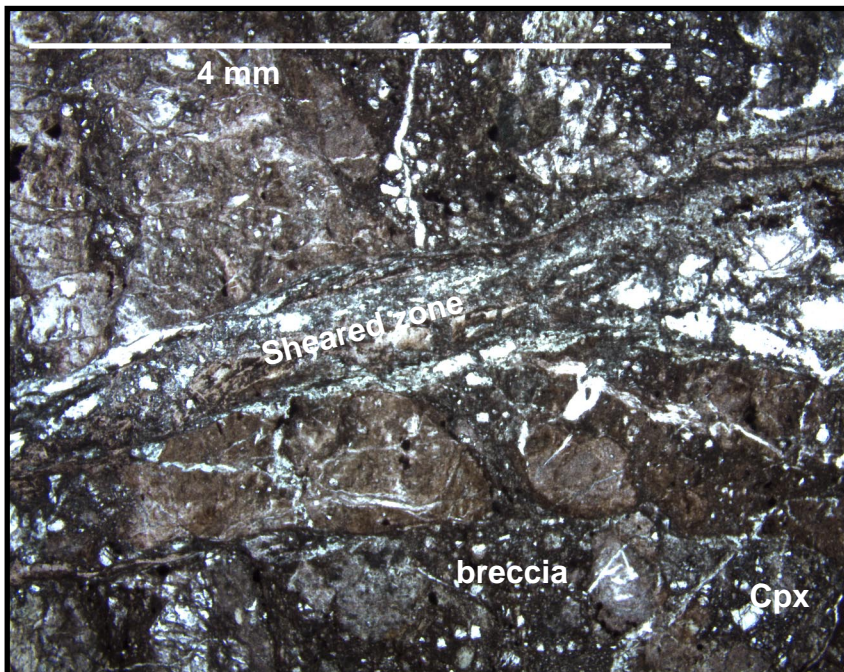


Figure F15. A. Hand specimen showing the network of veins (filled with quartz + epidote and quartz) fracturing the gabbro (Sample 180-1117A-12R-1, 26–35.5 cm). (Continued on next page.)

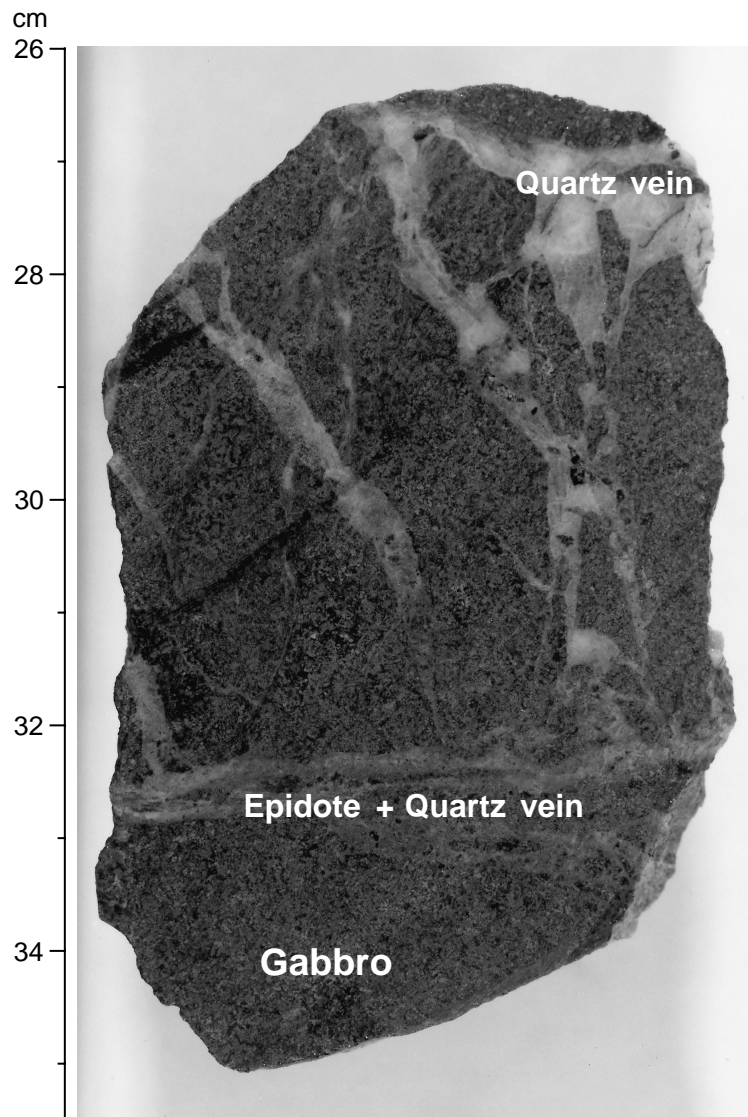


Figure F15. (continued). B. Thin section showing epidote + quartz (Ep, Qz) and quartz (Qz) veins crosscutting the brecciated gabbro (Sample 180-1117A-12R-1 [Piece 2, 6–8 cm]). Epidote + chlorite (Ep + Chl) replacing previous minerals in the matrix.

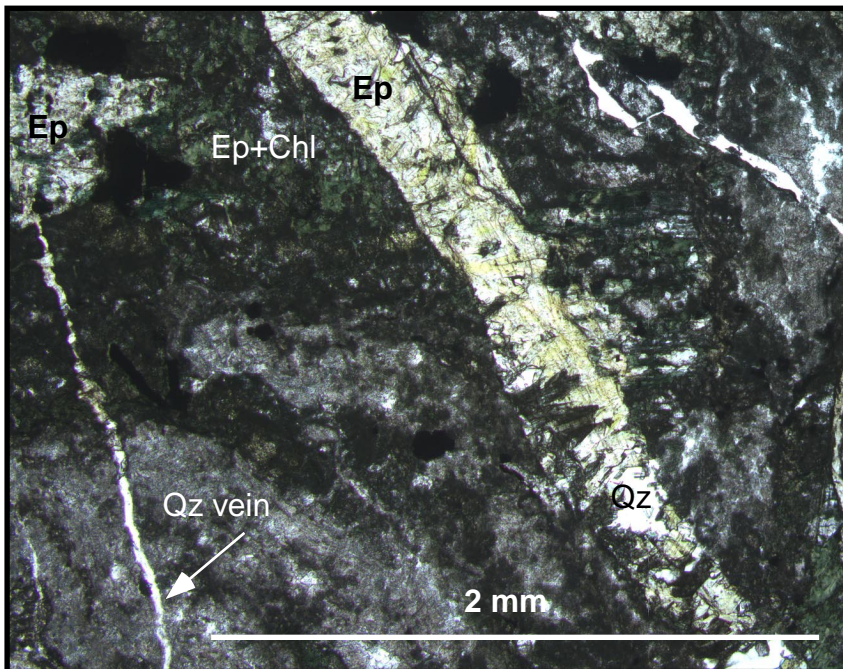


Figure F16. Fracturing of altered basic igneous rock during Si-rich fluid circulation (Sample 180-1117C-1R-1, 9–10 cm). Ep = epidote; Qz = quartz; and Qz vein = vein filled with quartz.

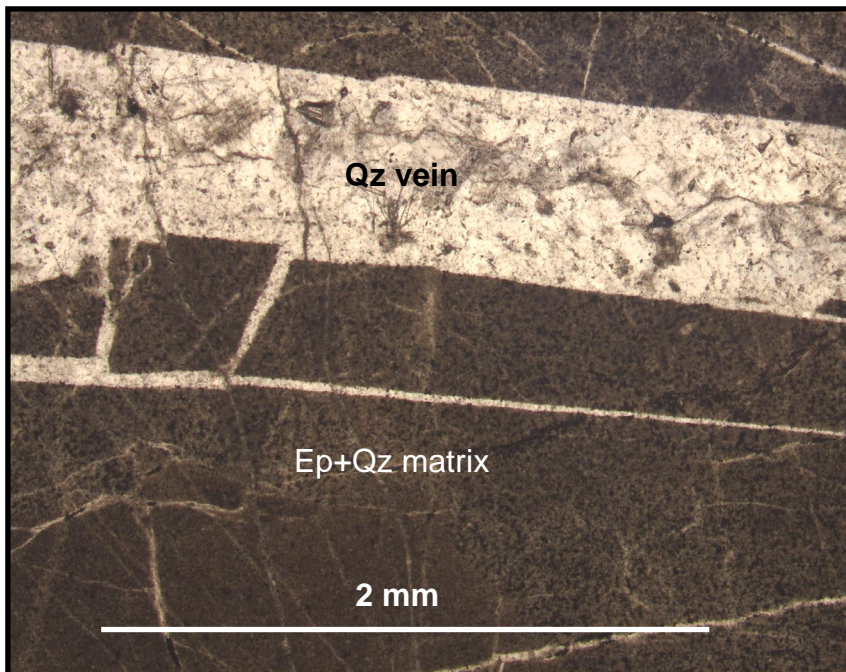
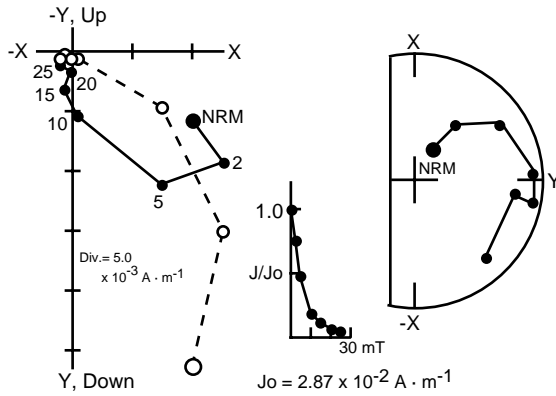
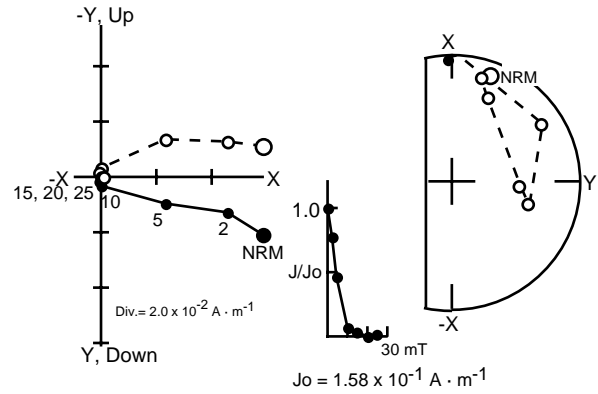


Figure F17. Demagnetization behavior of discrete samples from Site 1117. Vector plots: horizontal component = solid circles; vertical component = open circles; Div. = division. Stereonet plots: lower hemisphere = solid circles; upper hemisphere = open circles. **A.** Sample 180-1117A-1R-1, 20–22 cm (0.22–0.24 mbsf). **B.** Sample 180-1117A-2R-CC, 7–9 cm (12.27–12.29 mbsf). **C.** Sample 180-1117A-9R-1 (Piece 17). **D.** Sample 180-1117A-11R-1 (Piece 7). NRM = natural remanent magnetization; Div. = division; Jo = NRM intensity.

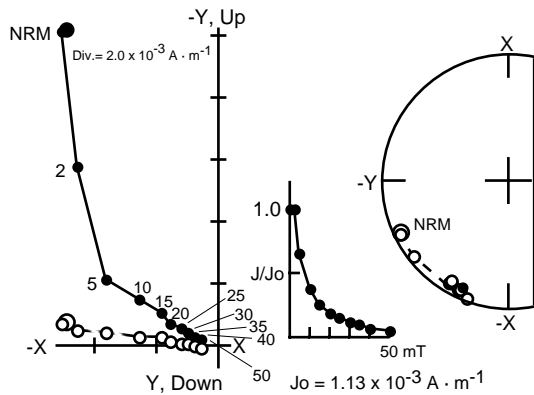
A 180-1117A-1R-1, 20-22 cm
[0.22 - 0.24 mbsf]



B 180-1117A-2R-CC, 7-9 cm
[12.27 - 12.29 mbsf]



C 180-1117A-9R-1, pc. 17



D 180-1117A-11R-1, pc. 7

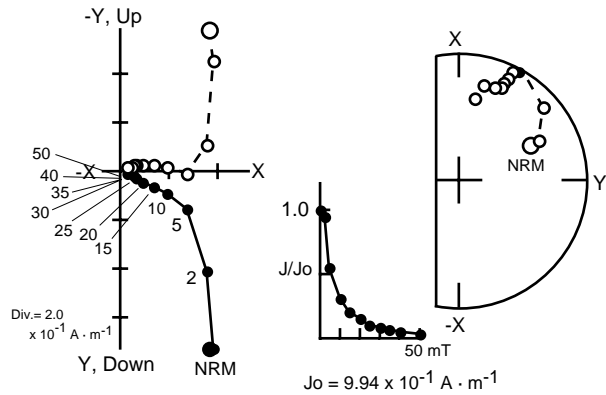


Figure F18. Plots of declination, inclination, and intensity for Core 180-1117A-1R. Data from long core sections after AF demagnetization shown as solid circles; data from discrete samples after AF demagnetization shown as open squares. A. After AF demagnetization at 20 mT. (Continued on next page.)

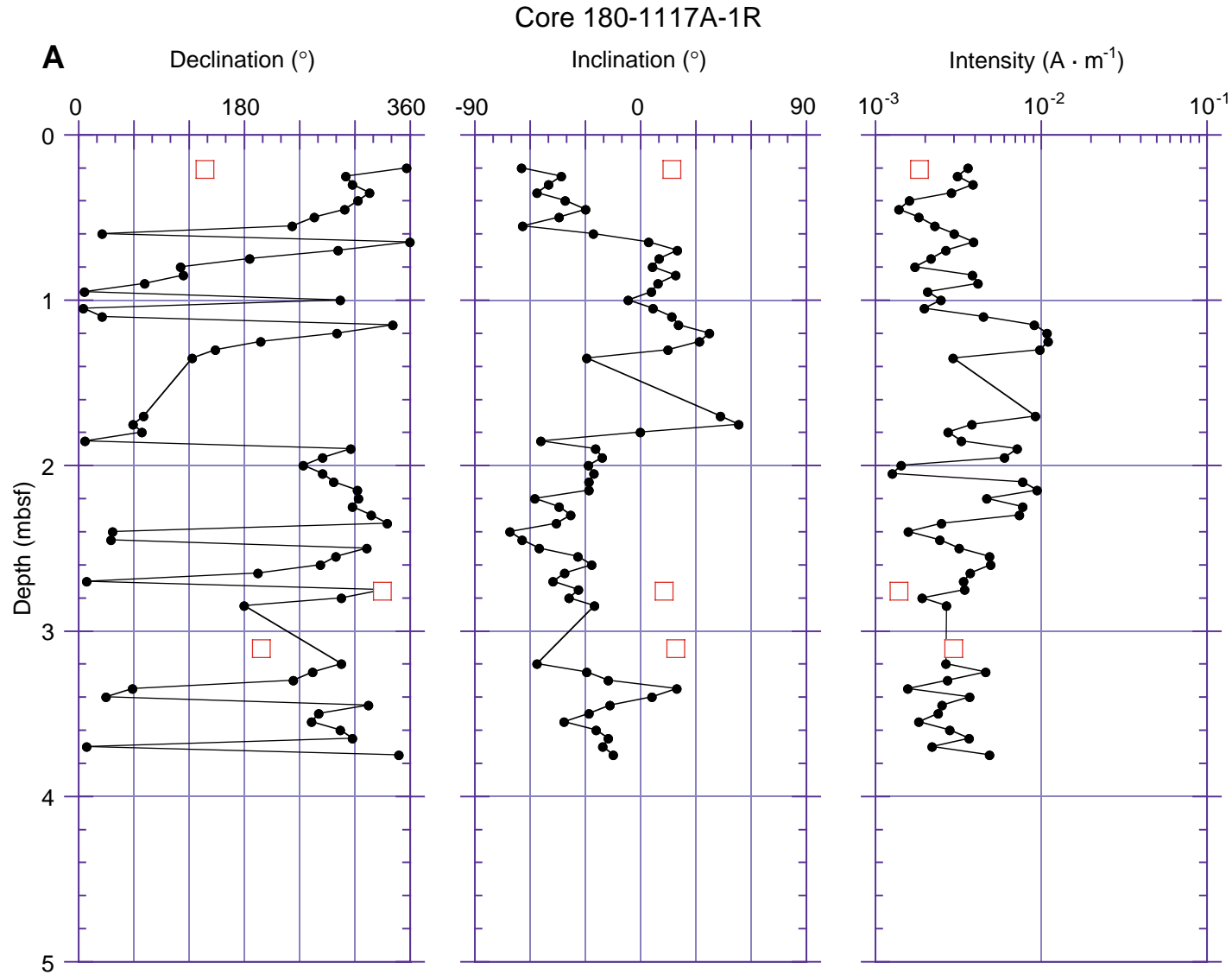


Figure F18. (continued) B. After AF demagnetization at 25 mT.

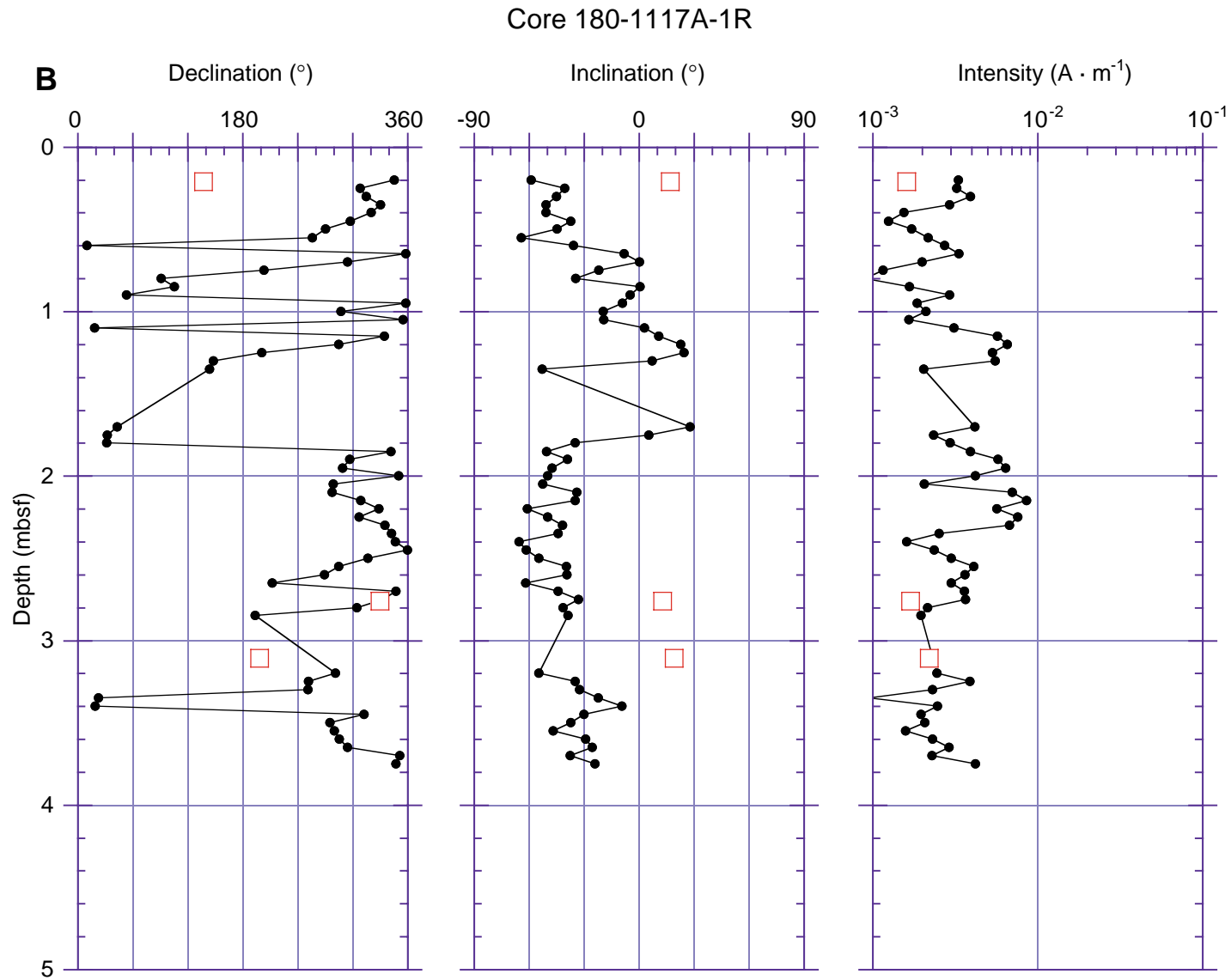


Figure F19. Susceptibility data from AMST measurements of long core sections, Core 180-1117A-1R.

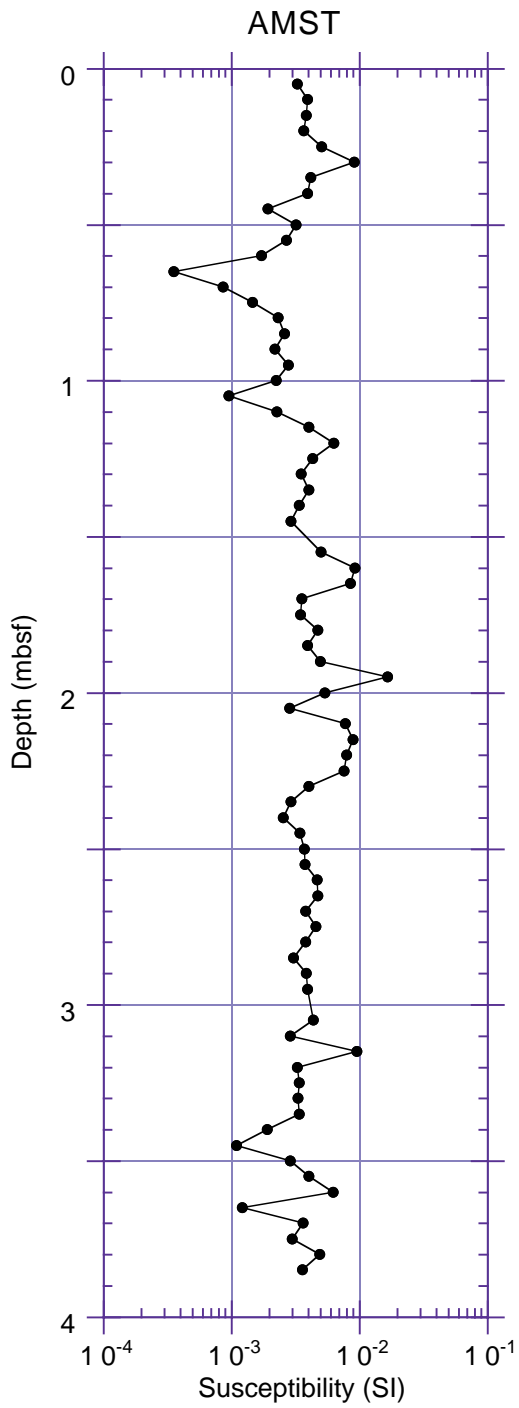


Figure F20. Rock magnetic data for discrete samples, Hole 1117A. **A.** Plot of AMS parameters P_j vs. T , calculated according to Jelinek (1981). **B.** Plot of the acquisition of isothermal remanent magnetization (IRM) vs. applied field (T = Tesla). **C.** Plot of the normalized decay of anhysteretic remanent magnetization (ARM) during AF demagnetization (mT = milliTesla; J = remanent intensity; and J_0 = initial intensity).

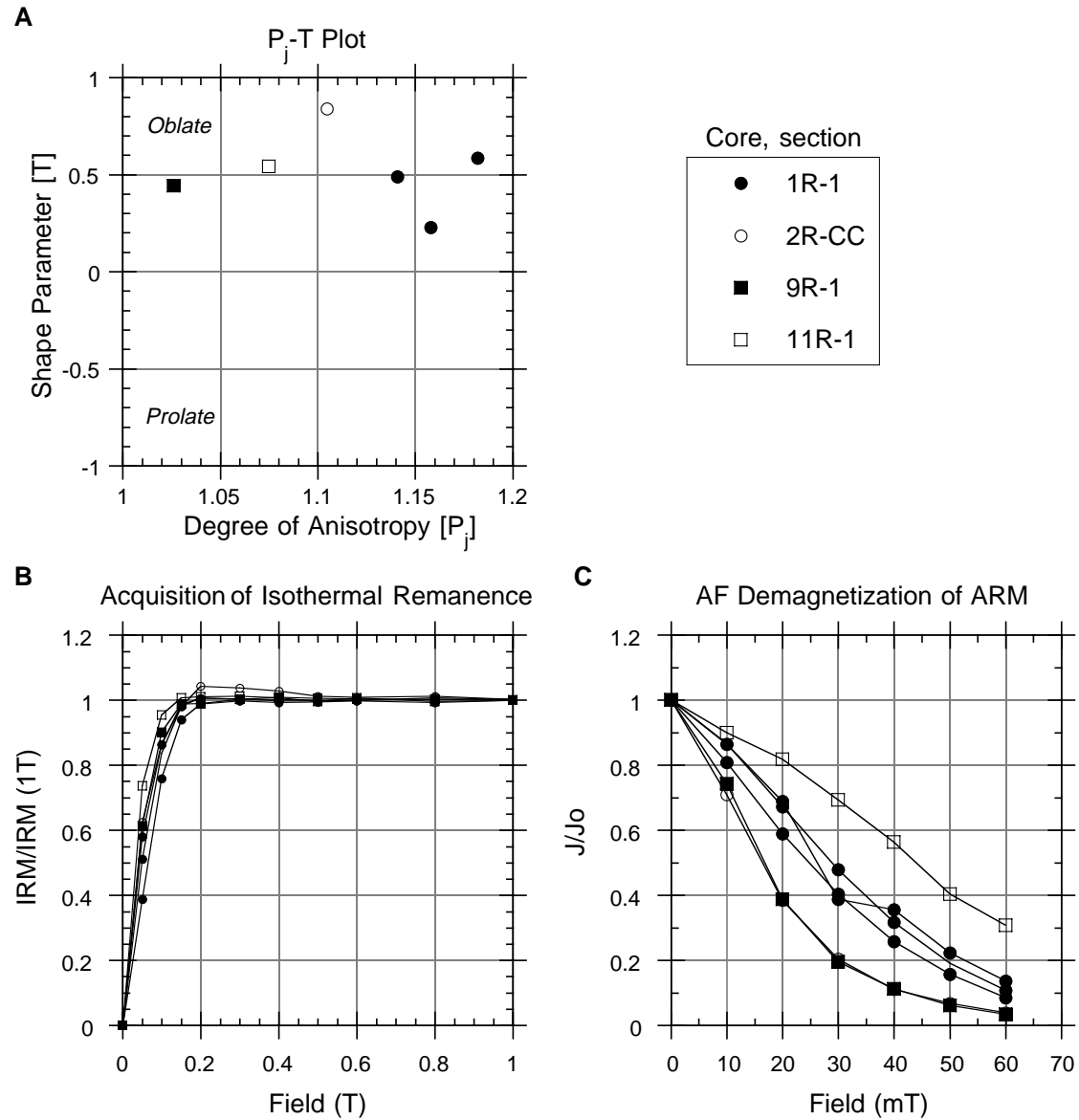


Table T1. Site 1117 coring summary. (Continued on next page.)

Hole 1117A

Latitude: 9°46.526'S
 Longitude: 151°32.945'E
 Seafloor (drill-pipe measurement from rig floor, mbrf): 1174.9
 Distance between rig floor and sea level (m): 11.70
 Water depth (drill-pipe measurement from sea level, m): 1163.2
 Total depth (from rig floor, mbrf): 1286.0
 Total penetration (mbsf): 111.1
 Total number of cores: 14
 Total length of cored section (m): 111.1
 Total core recovered (m): 6.42
 Core recovery (%): 6

Core	Date (July 1998)	Time (UTC +10 hr)	Depth (mbsf)	Length cored (m)	Length recovered (m)	Recovery (%)	Comments
180-1117A-							
1R	26	2215.0	0.0-12.2	12.2	4.07	33.4	
2R	27	330.0	12.2-18.6	6.4	0.17	2.7	
3R	27	635.0	18.6-28.2	9.6	0.04	0.4	
4R	27	800.0	28.2-37.8	9.6	0.00	0.0	No recovery
5R	27	1035.0	37.8-47.4	9.6	0.00	0.0	No recovery
6R	27	1240.0	47.4-57.0	9.6	0.00	0.0	No recovery
7R	27	1435.0	57.0-61.6	4.6	0.07	1.5	
8R	27	1605.0	61.6-66.6	5.0	0.12	2.4	
9R	27	1810.0	66.6-76.3	9.7	0.75	7.7	
10R	27	1940.0	76.3-85.9	9.6	0.16	1.7	
11R	27	2135.0	85.9-95.5	9.6	0.44	4.6	
12R	27	2355.0	95.5-105.2	9.7	0.36	3.7	
13R	28	150.0	105.2-110.0	4.8	0.15	3.1	
14R	28	425.0	110.0-111.1	1.1	0.09	8.2	
Totals:				111.10	6.42	5.8	

Hole 1117B

Latitude: 9°46.527'S
 Longitude: 151°32.951'E
 Seafloor (drill-pipe measurement from rig floor, mbrf): 1174.9
 Distance between rig floor and sea level (m): 11.7
 Water depth (drill-pipe measurement from sea level, m): 1163.2
 Total depth (from rig floor, mbrf): 1184.4
 Total penetration (mbsf): 9.5
 Number of cores: 1
 Total length of cored section (m): 9.5
 Total core recovered (m): 0.05
 Core recovery (%): 0.5

Core	Date (July 1998)	Time (UTC +10 hr)	Depth (mbsf)	Length cored (m)	Length recovered (m)	Recovery (%)
180-1117B-						
1R	28	0845	0.0-9.5	9.5	0.05	0.5
Totals:				9.5	0.05	0.5

Hole 1117C

Latitude: 9°46.520'S
 Longitude: 151°32.943'E
 Seafloor (drill-pipe measurement from rig floor, mbrf): 1174.9
 Distance between rig floor and sea level (m): 11.7
 Water depth (drill-pipe measurement from sea level, m): 1163.2
 Total depth (from rig floor, mbrf): 1184.4
 Total penetration (mbsf): 9.5
 Total number of cores: 1
 Total length of cored section (m): 9.5
 Total core recovered (m): 0.10
 Core recovery (%): 1

Table T1 (continued).

Hole 1117C

Core	Date (July 1998)	Time (UTC +10 hr)	Depth (mbsf)	Length cored (m)	Length recovered (m)	Recovery (%)
180-1117C- 1R	28	1140	0.0-9.5	9.50	0.10	1.1
Totals:				9.50	0.10	1.1

Note: UTC = Universal Time Coordinated.

Table T2. Site 1117 coring summary by section. (Continued on next page.)

Core	Date (July 1998)	Time (UTC +10 hr)	Core depth (mbsf)		Length (m)		Recovery (%)	Section	Length (m)		Section depth (mbsf)		Catwalk samples	Comments
			Top	Bottom	Cored	Recovered			Liner	Curated	Top	Bottom		
180-1117A-														
1R	26	2215	0.0	12.2	12.2	4.07	33.4							
								1	1.50	1.50	0.00	1.50	IW	
								2	1.50	1.50	1.50	3.00	HS	
								3	0.91	0.91	3.00	3.91		
								CC	0.16	0.16	3.91	4.07	PAL	
									<u>4.07</u>	<u>4.07</u>				
2R	27	0330	12.2	18.6	6.4	0.17	2.7							
								CC	0.17	0.17	12.20	12.37	PAL, HS	
									<u>0.17</u>	<u>0.17</u>				
3R	27	0635	18.6	28.2	9.6	0.04	0.4							
								CC	0.04	0.20	18.60	18.80		
									<u>0.04</u>	<u>0.20</u>				
4R	27	0800	28.2	37.8	9.6	0.00	0.0							No Recovery
								1	0.00	0.00				
									<u>0.00</u>	<u>0.00</u>				
5R	27	1035	37.8	47.4	9.6	0.00	0.0							No Recovery
								1	0.00	0.00				
									<u>0.00</u>	<u>0.00</u>				
6R	27	1240	47.4	57.0	9.6	0.00	0.0							No Recovery
								1	0.00	0.00				
									<u>0.00</u>	<u>0.00</u>				
7R	27	1435	57.0	61.6	4.6	0.07	1.5							
								1	0.07	0.08	57.00	57.08		
									<u>0.07</u>	<u>0.08</u>				
8R	27	1605	61.6	66.6	5.0	0.12	2.4							
								1	0.12	0.12	61.60	61.72		
									<u>0.12</u>	<u>0.12</u>				
9R	27	1810	66.6	76.3	9.7	0.75	7.7							
								1	0.75	1.20	66.60	67.80		
									<u>0.75</u>	<u>1.20</u>				
10R	27	1940	76.3	85.9	9.6	0.16	1.7							
								1	0.16	0.17	76.30	76.47		
									<u>0.16</u>	<u>0.17</u>				
11R	27	2135	85.9	95.5	9.6	0.44	4.6							
								1	0.44	0.55	85.90	86.45		
									<u>0.44</u>	<u>0.55</u>				
12R	27	2355	95.5	105.2	9.7	0.36	3.7							
								1	0.36	0.56	95.50	96.06		
									<u>0.36</u>	<u>0.56</u>				

Table T2 (continued).

Core	Date (July 1998)	Time (UTC +10 hr)	Core depth (mbsf)		Length (m)		Recovery (%)	Section	Length (m)		Section depth (mbsf)		Catwalk samples	Comments
			Top	Bottom	Cored	Recovered			Liner	Curated	Top	Bottom		
13R	28	0150	105.2	110.0	4.8	0.15	3.1							
								1	0.15	0.25	105.20	105.45		
									0.15	0.25				
14R	28	0425	110.0	111.1	1.1	0.09	8.2							
								1	0.09	0.17	110.00	110.17		
									0.09	0.17				
			Totals:		111.1	6.42	5.8							
180-1117B- 1R	28	0845	0.0	9.5	9.5	0.05	0.1							
								1	0.00	0.09	0.00	0.09		
									0.05	0.09				
			Totals:		9.5	0.05	0.5							
180-1117C- 1R	28	1140	0.0	9.5	9.5	0.10	1.1							
								1	0.10	0.20	0.00	0.20	PAL	
									0.10	0.20				
			Totals:		9.5	0.10	1.1							

Note: IW = interstitial water; HS = headspace; PAL = paleontology.

Table T3. X-ray diffraction identification of minerals in pristine fault gouge.

Core, section, interval (cm)	Description	Major (minor) minerals
180-1117A-		
1R-1, 7-8	Fault gouge	Chrysotile, antigorite
1R-1, 24-25	Fault gouge	Talc, chlorite, calcite
1R-2, 0-1	Fault gouge	Talc, chlorite, calcite
1R-2, 13-14	Fault gouge	Talc, chrysotile, calcite
1R-2, 52-53	Fault gouge	Talc, calcite, chrysotile (chlorite)
1R-2, 58-59	Fault gouge	Lizardite, calcite, talc
1R-3, 1-2	Fault gouge	Calcite, chrysotile, talc (chlorite)
1R-3, 71-72	Fault gouge	Ankerite, talc, chrysotile (chlorite)
2R-CC, 9-10	Fault gouge	Talc, calcite, chlorite (quartz, amphibole)

Table T4. X-ray fluorescence results for major elements, Holes 1117A and 1117C.

Core, section, interval (cm)	Sample	SiO ₂	Average	TiO ₂	Average	Al ₂ O ₃	Average	Fe ₂ O ₃	Average	MnO	Average	MgO	Average
180-1117A-													
9R-1, 85-86	1a	50.47		0.88		15.73		9.59		0.15		8.63	
	1b	50.71	50.59	0.88	0.88	15.68	15.71	9.49	9.54	0.15	0.15	8.70	8.67
11R-1, 32-35	2a	50.47		2.52		12.39		19.31		0.27		4.30	
	2b	50.55	50.51	2.53	2.53	12.44	12.41	19.34	19.33	0.27	0.27	4.35	4.33
12R-1, 11-13	3a	49.37		2.92		11.73		21.48		0.27		4.37	
	3b	49.20	49.29	2.97	2.95	11.57	11.65	21.72	21.60	0.28	0.27	4.36	4.37
14R-1, 4-7	4a	53.36		1.58		13.44		13.47		0.24		5.83	
	4b	52.86	53.11	1.56	1.57	13.41	13.43	13.60	13.53	0.24	0.24	5.81	5.82
180-1117C-													
1R-1, 9-10	5a	69.86		0.88		14.59		5.99		0.08		2.58	
	5b	69.54	69.70	0.87	0.87	14.52	14.55	5.95	5.97	0.08	0.08	2.58	2.58
Comparative analysis*	6		50.70		0.85		15.40		14.59		0.12		5.63

Notes: LOI = loss on ignition. Major element values are in weight percent; a and b = duplicate analyses of the same sample; * = Lippard et al., 1986, table 3.9, sample OM984.

Table T4 (continued).

Sample	CaO	Average	Na ₂ O	Average	K ₂ O	Average	P ₂ O ₅	Average	Total	Average	L.O.I.	Average	Rock type
1a	14.39		0.48		0.03		0.07		100.42		4.99		Chlorite-epidote schist
1b	14.46	14.43	0.44	0.46	0.03	0.03	0.07	0.07	100.59	100.50	4.99	4.99	
2a	8.43		2.88		0.17		0.20		100.95		1.85		Quartz gabbro
2b	8.44	8.43	2.77	2.83	0.17	0.17	0.19	0.19	101.06	101.01	1.85	1.85	
3a	8.72		1.92		0.15		0.17		101.09		1.46		Brecciated quartz gabbro
3b	8.71	8.71	1.98	1.95	0.15	0.15	0.16	0.17	101.10	101.09	1.46	1.46	
4a	10.29		2.78		0.23		0.10		101.33		2.09		Quartz gabbro
4b	10.19	10.24	2.77	2.77	0.23	0.23	0.11	0.11	100.78	101.73	2.09	2.09	
5a	1.84		4.32		1.41		0.12		101.68		1.44		Hornfels
5b	1.82	1.83	4.32	4.32	1.40	1.41	0.12	0.12	101.20	101.44	1.44	1.44	
6		10.23		1.64		0.04		0.05		99.90		1.46	Ferrogabbro from Samail ophiolite*

Table T5. X-ray fluorescence results for trace elements, Holes 1117A and 1117C.

Core, section, interval (cm)	Sample	Nb	Average	Zr	Average	Y	Average	Sr	Average	Rb	Average	Zn	Average
180-1117A- 9R-1, 85-86	1	3		40		15		22		1		69	
		3	3	39	39	12	13	24	23	1	1	66	67
11R-1, 32-35	2	10		102		35		88		3		116	
		10	10	101	101	34	35	89	89	3	3	115	115
12R-1, 11-13	3	8		84		31		97		3		117	
		8	8	84	84	29	30	99	98	3	3	117	117
14R-1, 4-7	4	6		69		24		115		4		83	
		6	6	68	69	24	24	118	117	4	4	81	82
180-1117C- 1R-1, 9-10	5		11		133		24		125	41	41		33
Comparative analysis*	6				19		14		103				39

Note: Trace element values measured in parts per million; * = Lippard et al., 1986, table 3.9, sample OM984.

Table T5 (continued).

Sample	Cu	Average	Ni	Average	Cr	Average	V	Average	Ce	Average	Ba	Average	Rock type
1	103		136		511		253		23		57		Chlorite-epidote schist
	104	103	134	135	513	512	250	251	29	26	61	59	
2	125		37		0		502		0		0		Quartz gabbro
	126	125	35	36	0	0	502	502	0	0	0	0	
3	301		41		0		795		0		0		Brecciated quartz gabbro
	297	299	39	40	0	0	811	813	0	0	0	0	
4	236		40		0		386		7		2		Quartz gabbro
	235	235	40	40	0	0	389	387	4	0	0	1	
5		24		82		77		108		40		118	Hornfels
6		87		26		26		802					Ferrogabbro from Samail ophiolite*

Table T6. Anisotropy of magnetic susceptibility (AMS) data of discrete samples, Hole 1117A.

Core, section, interval (cm)	Depth (mbsf)	Mean volume susceptibility ($\times 10^{-3}$ SI)	AMS parameters	
			P_j	T
180-1117A-				
1R-1, 20-22	0.22-0.24	7.373	1.141	0.489
1R-2, 125-127	2.75-2.77	5.770	1.182	0.584
1R-3, 10-12	3.10-3.12	5.983	1.158	0.230
2R-CC, 7-9	12.27-12.29	13.78	1.105	0.839
9R-1 (Piece 17)		0.5332	1.026	0.444
11R-1 (Piece 7)		63.33	1.075	0.542

Note: Degree of anisotropy (P_j) and shape parameter (T) calculated according to Jelinek (1981).

Table T7. Calcium carbonate, carbon, nitrogen, and sulfur contents, Hole 1117A.

Core, section, interval (cm)	Depth (mbsf)	Inorganic carbon (wt%)	CaCO ₃ (wt%)	Organic carbon (wt%)	Total nitrogen (wt%)	Total sulfur (wt%)
180-1117A-						
1R-1, 27-28	0.27	1.00	8.32			
1R-1, 135-136	1.35	0.57	4.78	0.12		0.04
1R-2, 28-29	1.78	0.96	8.00			
1R-3, 88-89	3.88	1.88	15.67	0.23		
2R-CC, 8-9	12.28	1.13	9.40			

Note: Blanks indicate values below detection limit.

Table T8. Physical properties measured in cores, Hole 1117A.

Leg	Site	Hole	Core	Type	Section	Top (cm)	Bottom (cm)	Depth (mbsf)	Water content (bulk)	Water content (dry)	Bulk density (g·cm ⁻³)	Dry density (g·cm ⁻³)	Grain density (g·cm ⁻³)	Porosity (%)	Void ratio	Compressive strength (kPa)	Velocity			Thermal conductivity (W·m ⁻¹ ·°C ⁻¹)	
																	(m·s ⁻¹)	(m·s ⁻¹)	(m·s ⁻¹)		
180	1117	A	1	R	1	27	34	0.27	—	—	—	—	—	—	—	—	—	—	—	1.75	
180	1117	A	1	R	1	27	34	0.27	—	—	—	—	—	—	—	—	—	—	—	—	1.65
180	1117	A	1	R	1	39	41	0.39	12.87	14.77	2.28	1.99	2.79	28.68	0.40	—	2032.90	—	—	—	—
180	1117	A	1	R	2	10	10	1.60	—	—	—	—	—	—	—	65.00	—	—	—	—	—
180	1117	A	1	R	2	38	40	1.88	15.04	17.70	2.20	1.87	2.77	32.33	0.48	—	1991.90	—	—	—	—
180	1117	A	1	R	2	65	65	2.15	—	—	—	—	—	—	—	70.00	—	—	—	—	—
180	1117	A	1	R	2	100	100	2.50	—	—	—	—	—	—	—	90.00	—	—	—	—	—
180	1117	A	1	R	2	130	130	2.80	—	—	—	—	—	—	—	85.00	—	—	—	—	—
180	1117	A	1	R	3	23	25	3.23	12.95	14.88	2.26	1.97	2.75	28.57	0.40	—	2037.90	—	—	—	—
180	1117	A	1	R	3	48	50	3.48	—	—	—	—	—	—	—	—	—	—	—	—	1.32
180	1117	A	1	R	3	48	50	3.48	—	—	—	—	—	—	—	—	—	—	—	—	1.34
180	1117	A	2	R	CC	6	8	12.26	17.81	21.68	2.14	1.76	2.80	37.18	0.59	—	—	—	—	—	—
180	1117	A	9	R	1	16	18	66.76	1.10	1.10	2.76	2.73	2.82	2.95	0.03	—	—	—	—	—	—
180	1117	A	9	R	1	16	19	66.76	—	—	—	—	—	—	—	—	—	—	—	—	1.48
180	1117	A	9	R	1	16	19	66.76	—	—	—	—	—	—	—	—	—	—	—	—	1.15
180	1117	A	9	R	1	80	82	67.40	—	—	—	—	—	—	—	—	6075.70	6432.30	6336.70	—	—
180	1117	A	11	R	1	30	33	86.20	—	—	—	—	—	—	—	—	—	—	—	—	2.05
180	1117	A	11	R	1	30	33	86.20	—	—	—	—	—	—	—	—	—	—	—	—	2.06
180	1117	A	11	R	1	35	37	86.25	—	—	—	—	—	—	—	—	6260.30	6284.00	5990.80	—	—
180	1117	A	12	R	1	26	35	95.76	—	—	—	—	—	—	—	—	—	—	—	—	3.79
180	1117	A	12	R	1	26	35	95.76	—	—	—	—	—	—	—	—	—	—	—	—	3.55
180	1117	A	12	R	1	42	56	95.92	—	—	—	—	—	—	—	—	—	—	—	—	2.91
180	1117	A	12	R	1	42	56	95.92	—	—	—	—	—	—	—	—	—	—	—	—	2.63
180	1117	A	12	R	1	42	56	95.92	—	—	—	—	—	—	—	—	—	—	—	—	2.69
180	1117	A	12	R	1	42	56	95.92	—	—	—	—	—	—	—	—	—	—	—	—	2.50

Note: This table is also available in ASCII format in the [TABLES](#) directory.